Along-strike segmentation of seismic tremor and its relationship with the hydraulic structure of the subduction fault zone

Gaspard Farge[1,2], Claude Jaupart[1]and Nikolai M. Shapiro[3]

[1]Université de Paris, Institut de Physique du Globe de Paris, CNRS, F-75005 Paris, France
[2]Department of Earth and Planetary Sciences, University of California Santa Cruz, Santa Cruz, California, U.S.A.
[3]Institut de Sciences de la Terre, Université Grenoble Alpes, CNRS (UMR5275), Grenoble, France

Key Points:

- In subduction zones, the intensity of temporal clustering and the periodicity of tectonic tremor are segmented along-strike
- We use a model of fluid circulation in the fault to show that segmentation of activity can be caused by variation of transport properties
- Concordance of tremor segments and subducting seamounts in Shikoku, Japan suggests that segmentation could be due to slab topography

Corresponding author: Gaspard Farge, gafarge@ucsc.edu

Abstract

Along the strike of subduction zones, tectonic tremor activity is segmented on a geologic scale, indicating local variations of the tremor-generating process. Here, we study how strong temporal clustering and long-term recurrence of activity can emerge from the synchronization of elementary tremor sources, as they interact through fluid pressure transients. We model tremor sources as rapid openings of low-permeability valves in the permeable fault zone channeling the upward flow of deep metamorphic fluids. Valve openings trigger fast pressure transients that generate seismic waves. In such a system, tremor activity is thus shaped by unsteady fluid circulation. Using numerical simulations of fluid flow for a large number of different valve populations, we show that the synchronized, collective activity of sources generates episodic activity, and that along-strike variations of fluid flux and fluid transport properties can lead to the segmentation of tremor activity. Strong tremor bursts that coherently activate wide parts of the fault and recur with a long period are associated with patches densely populated with valves and characterized by below-average permeability. Long-term tremor episodicity emerges from the synchronous activity of valves in such patches and is responsible for fluid-pressure cycling at the subduction scale. In the tremor zone of the Shikoku, Japan, subduction interface, the most temporally clustered segment coincides with a downgoing seamount chain, suggesting that the segmentation of the fault zone permeability, and hence of tremor activity, could be inherited from the topography of the subducting oceanic plate.

Plain Language Summary

In subduction, the fault zone controls plate convergence through friction, controlling if, when and where earthquakes occur. At depths larger than about 40 km, deformation in the fault vicinity transitions to a more stable, ductile regime. At those depths, no earthquakes are expected, and low-frequency tectonic tremor are detected instead. Geological and geophysical observations link tremor with the unsteady circulation of high-pressure fluid in the fault zone. Tremor could thus help understand how fluid flows along the subduction interface, where it acts to lower the fault strength and may therefore trigger seismic events. Tremor occurs intermittently, in bursts followed by quiet periods. In this study, we investigate the role of fluid circulation processes in generating tremor, and why its activity varies across different regions. In our model, the intermittence of tremor comes from the intermittence of fluid circulation in the fault. We describe how many small parts of the fault zone can interact, and open or close coherently, generating pulses of fluid flow and the observed bursts of tremor. This framework allows to interpret variations of tremor intermittence as a symptom of how strong the flow and how well fluid circulates in different parts of the subduction interface.

1 Introduction

1.1 Source processes of tectonic tremor and low-frequency earthquakes

In the deeper parts of subduction faults (at about 40 km depth), seismic signals with a lower frequency than earthquakes are detected in a wide frequency band ranging from 0.01 Hz to 10 Hz. Impulsive events called *low-frequency earthquakes* (LFEs) and *very-low frequency earthquakes* (VLFEs) are detected in the high (1–10 Hz) and low (0.02–0.05 Hz) frequency bands, respectively (Obara, 2002; Katsumata & Kamaya, 2003; Ito et al., 2007). *Tectonic tremor* is a long (10s to days), non-impulsive seismic signal in which LFEs and VLFEs are almost systematically detected, from the same localized sources (Rubin & Armbruster, 2013; Chestler & Creager, 2017). Tremor, LFEs and VLFEs appear to be systematically correlated with one another in space and time, suggesting that they are manifestations of the same broadband phenomenon in different frequency intervals (*e.g.* Masuda et al., 2020). In this study, we will study the collective, long-term patterns of LFE activity to understand their underlying physical processes. We will therefore use

the terms "tremor" or "tremor activity" as a synonym for LFE activity, considering that tremor is composed of many LFEs (Shelly et al., 2006; Ide, 2021) — although we recognize that this approach might gloss over potentially different source processes. Tremor activity is intermittent and proceeds in periods of intense activity formed of clusters of LFEs, separated by periods of quiescence (Obara, 2002; Rogers, 2003; Shelly et al., 2007; Brudzinski et al., 2010; Frank et al., 2014; Idehara et al., 2014). The temporal clustering of activity, the duration, sizes and recurrence timescales of tremor bursts vary between subduction zones. Bursts typically last from less than an hour to a week and are seperated by hours to months (*e.g.* Frank et al., 2014). Thus, the timescales of tectonic tremor activity can be several orders of magnitude longer than the average recurrence time and duration on an individual LFE.

The geological processes that generate tectonic tremor remain elusive. The strongest episodes of tremor slow-slip events (SSEs) on the fault interface (Obara et al., 2004; Rogers, 2003; Shelly et al., 2006; Frank, Radiguet, et al., 2015) and episodes of strong fluid pressure change in the source region (Frank, Shapiro, et al., 2015; Nakajima & Uchida, 2018; Tanaka et al., 2018; Warren-Smith et al., 2019; Gosselin et al., 2020). This hints at the occurence of cycles of accumulation and release of hydro-mechanical stress in the fault, a process first described by R. Sibson (1992) as *fault-valving*. As fluid is released dehydration reactions in the oceanic crust (Anderson et al., 1976), regions of low permeability above the slab can seal the interface, leading to high-pressure anomalies (Shelly et al., 2006; Calvert et al., 2011; Wannamaker et al., 2014). These lead to decreased effective normal stress on the fault, and slip can therefore nucleate with minor changes of the stress field. As the slip front propagates, fueled and stabilized by the high fluid pressures (Segall et al., 2010), the induced fracturing is likely to open fluid pathways, thereby lowering the local fluid pressure (Frank, Shapiro, et al., 2015). Tremor is thought to be generated during this phase. When the permeability around the fault heals, fluid pressure rises again, and a new cycle begins (R. Sibson, 1992).

The geological study of outcrops of paleo-subduction zones indicates that fluid pressures are indeed highly heterogeneous and variable, with evidence of supra-lithostatic pressures triggering vein-opening (Angiboust et al., 2015; Muñoz-Montecinos et al., 2021; Taetz et al., 2018; Tarling et al., 2021; Platt et al., 2018; Behr & Bürgmann, 2021). The radiation pattern of LFEs, VLFEs and tremor is at least in part consistent with shear slip along the fault interface (Ide et al., 2007; Royer & Bostock, 2014; Ide & Yabe, 2014; Imanishi et al., 2016), triggered by aseismic slow slip (Ando et al., 2010; Ben-Zion, 2012; Sammis & Bostock, 2021). The accumulation of geologic evidence of coupled deformation and fluid flow at the source scale suggests that LFEs are also possibly associated with fluid movement in the fault (Muñoz-Montecinos et al., 2021; Taetz et al., 2018). The sudden fluid mass advection could generate a single-force source on the matrix (Takei & Kumazawa, 1994), participating in the LFE wavefield with a radiation pattern hardly distinguishable from a double-couple owing to the small aperture of seismic networks in subduction zones (Shapiro et al., 2018; Ohmi & Obara, 2002). A similar model has been suggested by Ukawa and Ohtake (1987) to explain low frequency volcanic earthquakes that may be generated by a sudden acceleration of fluid that would result in a changing viscous shear force acting on the conduit walls and oriented parallel to the flow. In this hydraulic process, the LFE source duration is controlled solely by the fluid diffusivity of the permeable medium, and does not depend on event magnitude, which is consistent with observations in Cascadia and Guerrero, Mexico (Bostock et al., 2015; Farge et al., 2020). This key property does not hold in Japanese subduction zones, however, which led some authors to attribute it to an observational bias (Ide, 2019; Supino et al., 2020).

The very small magnitude of LFEs and restrictions on the number of seismic stations that can be used hamper a clear-cut diagnosis of LFE source mechanisms. Thus, we take a different approach and focus on the role fluid flow processes. In the R. Sib-

son (1992) valve mechanism, fault slip and changes of fluid pressure are coupled. The common acception is that abrupt pressure changes are triggered by seismic rupture but we shall argue that they could well be due to processes internal to the permeable fault zone. One key feature of LFE activity is that tremor bursts involve seismic sources of limited extent (hundreds of meters at most) and proceed over large distances (tens of kilometers), showing that some long-range interaction mechanism is at work. This has usually been attributed to slow-slip propagation but simple models of tremor and seismicity show that fluid-assisted interaction between neighbouring sources can also lead to long-range synchronization (Farge et al., 2021; Fukuda et al., 2022). The smallest patterns of LFE clustering last less than an hour, which is consistent with the operation of source-scale processes.

1.2 Segmentation of tremor intermittence in subduction zones

Tremor activity is segmented in subduction zones: the recurrence intervals and temporal clustering are variable along both the dip and strike of the fault. In many subduction zones, tremor activity is not evenly distributed and several segments with different time clustering characteristics can be delimited along the strike of the fault (Poiata, Vilotte, Shapiro, Supino, & Obara, 2021; T. Wang et al., 2018; Brudzinski & Allen, 2007; Husker et al., 2019). The geologic scale (tens to hundreds of kilometers) and permanence of such segmentation indicates that it is likely due to large-scale, structural heterogeneity in the fault zone (Brudzinski & Allen, 2007; Maury et al., 2018; Ide, 2010). Spatial variations of fault properties are likely to haffect the distribution of tremor through their influence on frictional stress and weakness (Nakajima & Hasegawa, 2016; Kano et al., 2018; Cattania & Segall, 2021). They are also bound to have an impact on the plate dehydration rate and on the magnitude of fluid escape away from the fault zone, and by way of consequence on fluid flow conditions (Audet & Bürgmann, 2014; Halpaap et al., 2019; Gosselin et al., 2020; McLellan et al., 2022). One can anticipate that the link between small individual events and segment-scale activity depends on the spatial distribution of seismic sources. If fluid circulation is a major control mechanism, however, the flow rate is also likely to be a key variable.

In this study, our aim is to investigate how tremor sources synchronize, and how they conspire to shape the observed temporal clustering of activity, long recurrence timescales, and coherence of activity over wide space scales. We focus our analysis on the role of the dynamics of permeability, fluid flux and fluid pressure in the fault zone. We build upon an earlier study of along-dip fluid circulation in a dynamically permeable fault zone, where low-permeability plugs open and close in a valve-like manner (Farge et al., 2021). The valve mechanism simulates local changes of permeability and fluid pressure that may be associated with LFE source processes. We have previously shown that in such a system, realistic, tremor-like patterns of activity emerge due to the dynamics of fluid pressure.

In the present work, we systematically explore how the hydraulic forcing (the input fluid flux) and the distribution of low-permeability valves in control the intermittence of seismicity. The article is organized as follows. *(1)* We describe a new method to characterize the temporal clustering and recurrence timescales of LFE activity. We apply this method to characterize the segmentation of tremor intermittence in Shikoku, Japan. *(2)* We summarize key aspects of the valve model and the hydraulic and seismic behavior it produces. *(3)* We explore the interaction between two permeability valves. We show that its strength is controlled by the input fluid rate as well as the valve separation. *(4)* In a fourth part, we systematically explore how the spatial distribution of valves — their number and spatial clustering — and the input flow rate set the intermittence of tremor activity. Using more than 42,000 simulations, we show that both fluid flux and permeability structure determine the strength of long-range interactions, and hence how synchronized the activity is. *(5)* In a last part, we elaborate on the physical

origin of tremor activity segmentation in the Shikoku (Japan) subduction zone. We end the paper with a discussion of the scope and limitations of our model.

2 Characterizing tremor intermittence

2.1 Clustering and characteristic timescales of LFE activity

Tremor activity can be described in two complementary ways: either through a continuous prism by measuring how long or how often a tremor source is active in time, or through a more discrete *point process* description, looking at the occurrences of individual events, LFEs. In a point process description of the activity, LFEs occur in a "bursty" manner, with very short and very long inter-event delays much more probable than in a constant-rate, Poisson process (Goh & Barabasi, 2006). They form *clusters* of rapid LFE occurrences (sub-hourly delays), separated by long, quiet periods (one event per day or less) (Frank et al., 2014). LFE clusters — *i.e.* tremor bursts — last between an hour and a week. Similarly to LFEs, their occurrences cluster in time, more likely occurring soon before or after another burst. The degree of temporal clustering of activity varies between subduction zones, and between segments of a subduction zone. Some zones can exhibit an extremely clustered activity in time, with almost no background seismicity, and larger, less frequent bursts dominating the activity, while other regions can produce less clustered, more continuous activity, formed of smaller, shorter, more frequent bursts. Single bursts of activity can be spaced by a few hours in the most active periods, which recur on the scale of months to years. This superimposition of timescales of recurrence — individual events, clusters, clusters of clusters, etc — is characterized as a "scale-free" phenomenon by many studies (Idehara et al., 2014; Frank et al., 2016; Poiata, Vilotte, Shapiro, Supino, & Obara, 2021). However, when looking at the largest bursts of activity in a given region, one or several characteristic timescales of recurrence can be estimated. In the tremor zone of Guerrero (Mexico) for instance, the largest tremor bursts, associated with large (geodetic magnitude M7.5) SSEs recur every 4 to 5 years (Radiguet et al., 2012). Smaller bursts occur every three months or so, activating smaller parts of the fault, associated with M6.4 SSEs (Frank, Radiguet, et al., 2015; Frank & Brodsky, 2019). (Ide & Nomura, 2022) proposed a systematic characterisation of long-term and short-term recurrence of tremor episodes in the Nankai subduction zone, highlighting periods of 10–100 days and 1–10 hours.

2.2 The segmentation of LFE activity in Shikoku

In Figure 1e, we represent the LFE activity in time along the strike of the Shikoku tremor zone, in Japan (catalog from Poiata, Vilotte, Shapiro, Supino, & Obara, 2021). Three zones with different clustering and recurrence behavior can be visually identified, from least to most temporally clustered: zone 1, the westernmost part between 50–140 km along strike, zone 2, the easternmost part between 190–250 km along strike, and zone 3 in between, 140–190 km. In zone 1, activity is characterized by a relatively low level of temporal clustering, and a high background rate of events. Bursts are frequent, and recur on timescales of 2–3 months, although with a strong variability. In the easternmost zone, activity is more clustered, and bursts are slightly less frequent, recurring every 3 months in the eastern and western halves of the zone. Finally, in the boundary region between the two previous zones, the activity is least intense, with a very low background rate. Most of the events occur during large transients of activity which occasionally cross it, every 6 months to slightly less than a year. It is the most temporally clustered activity of the three regions. In other subduction zones, similar variations of temporal clustering and recurrence timescales can be observed, showing a clear along-strike segmentation of tremor activity. In the supplementary materials, we show time series of tremor activity rate in the Central American subduction zone (Figures S1, tremor log from Husker et al. (2019)) and along the Cascadia subduction zone (Figure S2, tremor catalog from

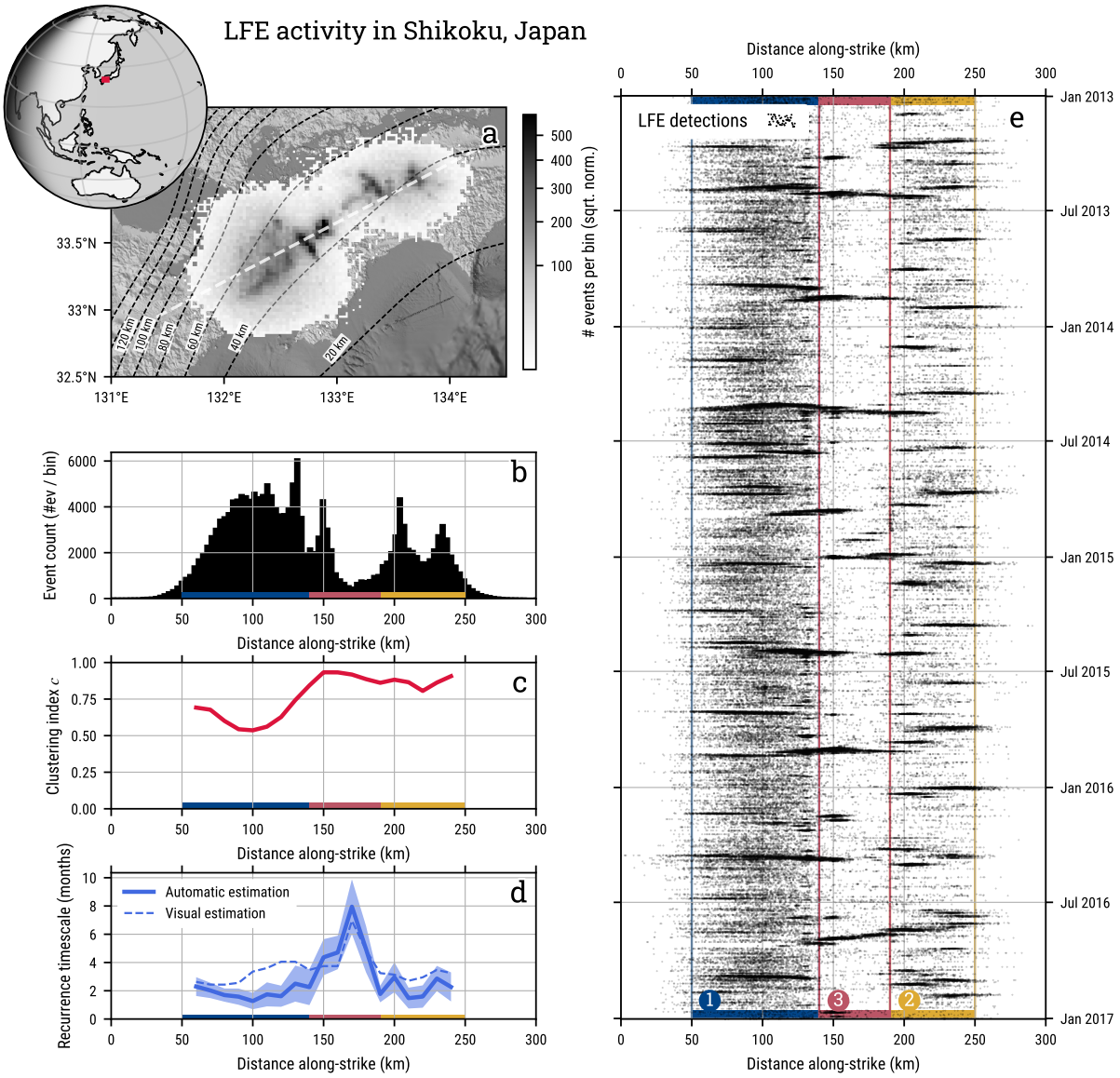

Figure 1: Caption on next page.

Figure 1. *On previous page.* Patterns of temporal clustering and recurrence of LFE activity, in Shikoku, Japan (2013–2017). *(a)* 2D histogram of LFE activity in 2.7 km by 2.7 km horizontal bins, colored according to the number of sources projected onto the surface (catalog from Poiata, Vilotte, Shapiro, Supino, and Obara (2021)). Depth contours of the slab from Slab2 (Hayes, 2018). The dotted white line indicates the along-strike direction. *(b)* Event count binned in 3-km wide bins along-strike, for the full period. *(c)* Intensity of temporal clustering along-strike, measured by the clustering index c in bins of 20 km, with a 10 km overlap. *(d)* Recurrence timescale of clusters along strike, with the same spatial bins as in *(c)*. Details on the cluster detection and clustering index can be found in Section 2.3. The blue, shaded area around the measurement represents 1-σ interval around the estimated recurrence timescale. A visually estimated recurrence is shown as a dotted blue line. *(e)* LFE activity along-strike in time, each black dot represents an event. Three major segments are highlighted in blue (zone 1), yellow (zone 2) and red (zone 3). See text for details, and Figure 12 for wider geographical context.

Wech and Creager (2008)). In Shikoku, Guerrero, and Cascadia, the segments are of geological scale, spanning tens to hundreds of kilometers along the strike of the subduction.

In all examples presented here (Shikoku in Figure 1, Guerrero in Figure S1 and Cascadia in Figure S2), the variations of temporal clustering, regularity of the recurrence and timescale of recurrence seem to be correlated: the stronger the clustering, the longer and more regular the recurrence, and therefore the more periodic the activity. In the light of this, large clusters, quasi-periodic behavior and long recurrence intervals can be interpreted as effects of the *synchronization* of the activity of tremor sources through physical interactions between them. Given a constant rate of activity for many sources, the stronger the synchronization between them, the more likely events are to occur within clusters, the larger the clusters, and therefore the longer their recurrence times. Measuring synchronization through temporal clustering and the timescale and regularity of the recurrence of activity therefore provides important insight into the physical mechanisms that allow tremor sources to interact, and shape their collective behavior.

2.3 Clustering and recurrence analysis

In order to study the synchronization of LFEs in models and observations, we design simple measures of the level of clustering of activity, and of timescales of recurrence of clusters of activity, and how variable they are. Those measures are based on an explicit detection of clusters, to avoid the ambiguity of spectral measurements — based on autocorrelation or Fourier analysis of activity time series for instance (*e.g.* Beaucé et al., 2019) — regarding which specific patterns the measured timescales are related to. The measures and algorithm are designed to be used automatically and with minimal tuning on both real and simulated catalogs of events, with a focus on being able to characterize both relatively constant and very clustered activity. This will allow us to gain a direct understanding of the characteristics of synthetic seismicity for large batches of simulations (several tens of thousands), with no changes of parameters.

The first measure is a temporal clustering index c, which quantifies the extent to which events occur within clusters, rather than as a more homogeneous process in time. To do so, we measure the proportion p_{ev}^{peaks} of events occurring during "peaks" in the time series of event counts — the number of events per time bin δt. Peaks of activity are defined as all consecutive bins in which the event count is higher than 66% of the time — following a similar methodology as Frank, Shapiro, et al. (2015) for LFE burst detection. Peaks therefore cover about 34% of the time period. For a constant activity

rate (for instance a Poisson process), events are homogeneously distributed in time, thus about 34% of the events occur during peaks. If the activity is clustered, events occur mostly during peaks, and p_{ev}^{peaks} is higher than 34%. The clustering index c is constructed by mapping linearly the proportion of events in peaks p_{ev}^{peaks} to 0–1:

$$c = \frac{p_{ev}^{peaks} - 0.34}{1 - 0.34} \tag{1}$$

If 100% of events are in peaks, events occur only in clusters and $c = 1$. If only 34% of events occur in peaks, events are more or less as likely to occur in peaks as outside of peaks, the activity is not clustered and $c = 0$. Figure S4 and Section 2 of the supplementary materials illustrate and describe this step of the analysis in more details.

In a second step, we measure the characteristic timescales of recurrence and their regularity. We perform this analysis only if the activity is temporally clustered, when $c > 0.25$ — *i.e.* more than 50% of events are in peaks. To do so, we design an automatic identification of clusters of events in time, based on the proximity of their occurrence times t_i. Clusters of events are detected using a density-based clustering algorithm (DBSCAN, (Ester et al., 1996), *scikit-learn* implementation (Pedregosa et al., 2011)). Clusters of events are then classified according to the number of events that make them up, using DBSCAN on cluster population size. In some cases, more than one characteristic size of clusters can be detected, and recurrence timescales should be measured only for a given size of cluster. Measuring the average of inter-cluster time intervals can give an estimation of the characteristic timescale of recurrence for a given class of clusters, and the ratio of the standard deviation to the average of inter-cluster times gives an estimate of how variable or regular the recurrence is.

By explicitly detecting clusters, and classifying them by size, we implicitly assume that the clustering of activity exhibits characteristic scales of cluster size, duration or recurrence delay, which is not always the case for LFE activity (Idehara et al., 2014; Frank et al., 2016; Poiata, Vilotte, Shapiro, Supino, & Obara, 2021), or intermittent microseismic activity in general (Beaucé et al., 2019, 2022), where scale-free behavior is often observed. The algorithm is tailored to focus on the longest timescales of recurrence, that is on the largest clusters of activity detected in a time series, which is in itself a characteristic scale of the system producing the activity.

We apply this method to the activity in Shikoku, to compute the clustering index c (Figure 1c), the recurrence timescale and its variability (Figure 1d). The automatic measurements are performed for the whole period (2013–2017), in bins of 20 km along strike, with 10 km overlap. The segmentation in three zones that we established visually using the time-dip representation of activity (Figure 1e) is confirmed by the automatic measurements: zone 1 produces the least clustered activity ($c \approx 0.6$), with the most frequent bursts (about every 2 months), zone 2 produces slightly less frequent bursts (about every 3 months), and an activity that is overall more clustered ($c \approx 0.8$), and zone 3 (140–190 km) produces the most clustered activity ($c \approx 0.9$), with the longest timescales of recurrence (around 6 months). This novel method therefore produces accurate and simple measures of intermittency of real patterns of seismicity, and its efficiency will be most useful to characterize synthetic activity for large batches of simulations, later in this study.

3 Model description

3.1 A valve model to describe fault zone permeability

Many geophysical measurements (*e.g.* Peacock et al., 2011; Audet & Kim, 2016; Wannamaker et al., 2014; Rubinstein et al., 2009) reveal that the regions of the fault zone where tremor originates has a high porosity and is saturated with fluid at near-lithostatic pressures. The fluid is mainly composed of supercritical water, freed from local dehy-

dration reactions of the oceanic plate minerals (Tarling et al., 2019), or originating from deeper sources and then channeled along the fault zone to the tremor source region (Hyndman et al., 2015; Taetz et al., 2018). Because of a strong contrast of permeability between the fractured fault zone and the overriding plate (Evans et al., 1997; Audet & Kim, 2016), fluid is trapped and channeled along the plate interface, preferentially along channels of high permeability (Piccoli et al., 2021; Eymold et al., 2021; Angiboust et al., 2014; Ague, 2014). Updip of the tremor source region, fluid can partly escape the plate interface through fracture networks in the overriding plate, or at the root of the accretionary wedge (Hyndman et al., 2015), allowing the pressure to drop slightly from lithostatic levels. As thoroughly detailed in Farge et al. (2021), Section 3, we describe fluid circulation processes in a one-dimensional, high-permeability channel along the dip of the fault zone, saturated with high-pressure fluid. This channel is fed at its deep end by a constant metamorphic fluid flux q_{in}, and is bound by a constant fluid pressure at its outer end, where it outputs to a highly connected fracture network towards the surface. We represent this system in Figure 2a and b. In a fluid-saturated porous medium, Darcy's law dictates that the mass flux of fluid per unit area of channel cross-section $q(x,t)$ is proportional to the local gradient of fluid pressure $p(x,t)$ along dip, and to permeability $k(x,t)$:

$$q(x,t) = -k(x,t) \times \frac{\rho\phi}{\eta} \times \frac{\partial p}{\partial x}(x,t) \tag{2}$$

where η is the fluid viscosity, ρ the fluid's density, ϕ the fault zone porosity. The fluid pressure $p(x,t)$ evolves along the dip of the channel x in time t according to a diffusion equation:

$$\frac{\partial p}{\partial t} = \frac{\partial}{\partial x}\left(D(x,t)\frac{\partial p}{\partial x}\right) \tag{3}$$

with a diffusivity

$$D(x,t) = \frac{k(x,t)}{\eta\beta\phi}, \tag{4}$$

where β is a composite, fluid-matrix compressibility.

In the tremor source region, the combination of a constant fluid input and low-permeability seal over the fault zone creates the near-lithostatic fluid pressure. Along the fault-zone channel, permeable segments filled with high pressure fluid are separated by impermeable barriers, caused by the fault-zone heterogeneity in grain/block size, fracture density, thickness of the permeable zone. At equilibrium, the heterogeneous distribution of permeability results in a decrease of fluid pressure in steps towards the surface along the dip of the fault (Gold & Soter, 1985; Shapiro et al., 2018). Because the input fluid flux in the fault zone is a constant stressing rate, the fluid pressure can progressively overcome the lithostatic burden just downdip of permeability barriers, forcing the dynamic opening of permeability (Hubbert & Willis, 1957; Etheridge et al., 1984; R. H. Sibson, 2017), and the fluid influx and rapid fluid pressure adjustment observed with both geophysical and geological means, at the source (Muñoz-Montecinos et al., 2021; Taetz et al., 2018) and subduction scale (Angiboust et al., 2015; Warren-Smith et al., 2019; Gosselin et al., 2020; Nakajima & Uchida, 2018; Tanaka et al., 2018). The dynamic opening of permeability could occur because of various mechanisms: hydraulic fracturing caused by the pressure difference across a barrier generating a force overcoming the rock's cohesive strength, opening of tensile cracks as fluid pressure overcomes the lithostatic burden (Hubbert & Willis, 1957), or dilatant slip triggered by the reduced effective normal stress on friction surfaces (Mitchell & Faulkner, 2008). After a rapid opening of permeability and relaxation of the fluid pressure, the permeability heals shut through a combination of clogging by cataclastic grains carried in the fluid (Candela et al., 2014), and mechanical and chemical cementation of fractures (*e.g.* Yasuhara & Elsworth, 2008). At the P-T conditions of the tremor source region, hot-pressing experiments suggest that even chemical healing could occur on the scale of days or less (*e.g.* Giger et al., 2007).

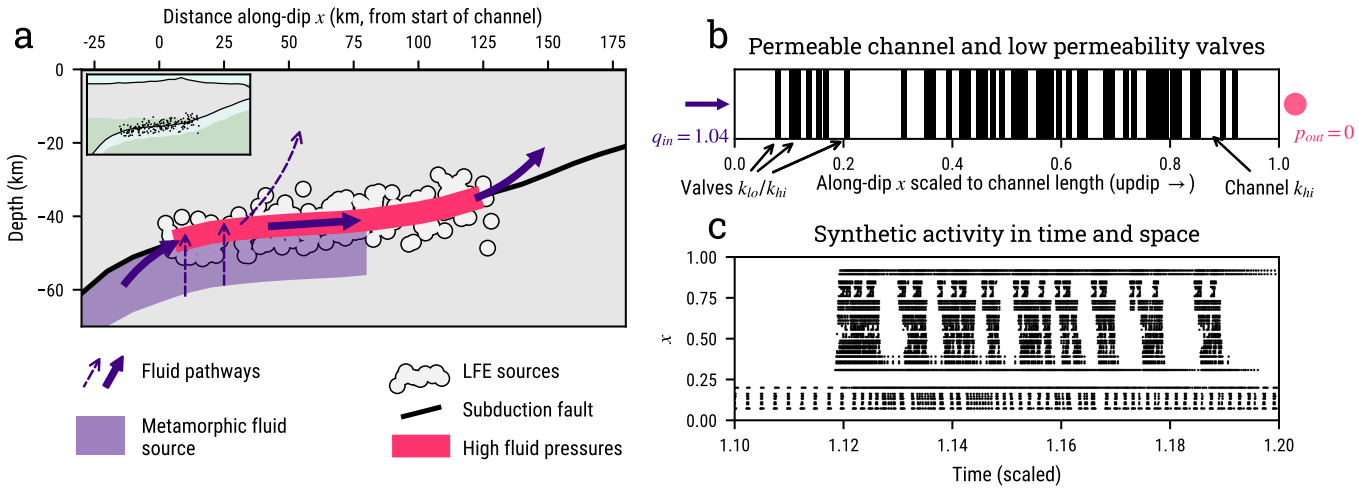

Figure 2. *(a)* Conceptual representation of fluid circulation in the fault zone. Downdip and below the tremor source region, metamorphic dehydration reactions release fluid, which is channeled in the permeable subduction interface, circulating at high fluid pressures. *(b)* Schematic representation of the model set up: a 1D permeable channel in which identical valves are distributed (black bars), opening and closing in response to the fluid pressure field. The channel is fed at its base by input fluid flux q_{in}, which is the main control parameter of the experiment. At its top, the channel is connected to a high permeability region such that the fluid pressure is close to the hydrostatic pressure $p_{out} = 0$ (see text for details on the scaling of physical properties). *(c)* Each valve opening is associated with a seismic event, a model LFE. The activity is represented in a space-time graph, with time on the x-axis, and distance along the channel on the y-axis. Figure reproduced and modified from Farge et al. (2021).

In our model, the small-scale heterogeneity of permeability in the channel is represented in a discrete, binary manner: short segments of the channel have a lower permeability k_{lo} than the surrounding $k_{hi} = \lambda k_{lo}$ ($\lambda << 1$), as represented in Figure 2b. The low-permeability segments behave as *valves*. We represent the opening of those segments in a simple manner: when the pressure difference δp across them exceeds a threshold δp_c^{break}, they instantly change to an open state, and their permeability switches to k_{hi}. When the accumulated overpressure across a now-open valve diffuses and δp drops below a lower threshold δp_c^{clog}, the valve then closes instantly, and the permeability in the segment goes back to k_{lo}. We do not model in details the dynamics either of the opening or closing of permeability. Although simply parameterized, they are based on a consistent modeling of how porous media clogs and unclogs in response to flux, pressure gradient and pore sizes when a particle-laden fluid circulates in it (Jäger et al., 2017; Bianchi et al., 2018; Souzy et al., 2020; Candela et al., 2014). More details on the modeling and its consistency can be found in Farge et al. (2021).

A key aspect of the model is that the along-dip width of the valve w_v is chosen arbitrarily, as the smallest scale of permeability heterogeneity we describe. Indeed, valves are elementary, dynamic segments of permeability, and we have shown in a previous study that their interactions seem to be creating *macro-valves*: segments of the channel of larger width, with a similar valving behavior (Farge et al., 2021). Here, our goal is to understand what controls this phenomenon, and how it affects the characteristics of seismic activity in the fault zone. The valves we use should therefore be thin enough that the effects on the seismicity are dominated by their collective behavior. Their width is set

at a hundredth of the channel length along-dip, to be convenient for our numerical approach. In essence, each elementary valve can however be composed of many smaller valving segments, resulting in a macro-valve of scale w_v.

In the model, permeability k changes occur without changes in porosity ϕ, which can occur if changes occur mostly to pore throats, changing the connectivity between pores (Steinwinder & Beckingham, 2019). Permeability is therefore the only control on fault zone transport properties in our model. All physical variables are scaled to characteristic values for our system: $x = 1$ is the length of the channel, $k = 1$ is the open permeability of the channel, $t = 1$ is the diffusive timescale across the channel when it is fully open, a unit of fluid pressure p corresponds to the lithostatic burden over the depth of the channel, a unit of fluid q corresponds to the flux obtained when a fluid pressure gradient of $\Delta p/\Delta x = 1$ is applied to the channel.

We assume that each valve opening is associated with an elementary tremor event, *i.e.* an LFE, emitted from the position of the valve, at the time of opening. It simulates the opening of permeability that is presumably associated with an LFE triggered by locally-high fluid pressure, trough a rupture, unclogging, or hydrofracture-like event (*e.g.* Kotowski & Behr, 2019; Shapiro et al., 2018; Muñoz-Montecinos et al., 2021). The cumulated activity of those synthetic LFEs could build up into signals that could be detected as large magnitude LFEs, VLFEs, and tremor. This description is simplistic, but our focus is not on an accurate physical description of the source of LFEs, VLFEs or tremor, but rather on the sensitivity to and effect on the fluid pressure field of elementary tremor sources, that allows source-to-source interaction.

In practice, we built and optimized a stable, accurate algorithm to solve the diffusion equation, compute fluid flux, valve state and therefore permeability throughout the channel (Farge et al., 2021). The main control parameters of this system are the value of the input fluid flux q_{in}, and the valve distribution in the channel. We retrieve a catalog of valve openings, which we consider to be an analog of LFE catalogs. Figure 2c displays the activity in time and space emitted by valves in a channel, as fluid is forced through it. To our knowledge, this model is the first to explicitly and causally describe the link between the hydraulic dynamics in the fault zone and the activity of tremor in time and space, opening a rich scope of exploration.

3.2 Valve behavior for different values of the input flux

Closed valves act as barriers to fluid flow in the channel, and as they impede the flow in the channel, the pressure difference across them can increase to the point they break. However, the fluid input rate q_{in} into the system controls if a valve can break open when closed, and close when open. Two threshold flux values can be derived from the δp thresholds, using Darcy's law for the flux through a valve in a permanent regime. The flux needed to reach the breaking threshold δp_c^{break} when a valve is closed is:

$$q_c^{break} = \frac{\rho}{\eta} k_{lo} \frac{\delta p_c^{break}}{w_v}, \tag{5}$$

where w_v is the valve's width. Therefore, when $q_{in} > q_c^{break}$, δp across a closed valve will eventually go over δp_c^{break}, and the valve will open. As the valve opens, the steep pressure gradients diffuses and δp drops across the valve. For the valve to close back, the strength of the flux has to allow δp to drop below the closing threshold δp_c^{clog}, and therefore q_{in} has to be lower than:

$$q_c^{clog} = \frac{\rho}{\eta} k_{hi} \frac{\delta p_c^{clog}}{w_v}. \tag{6}$$

In the previous equations, δp_c^{break} and δp_c^{clog} are defined as the difference of pressure from down- to updip of the valve, hence a different sign convention than equation 2. It is intuitive that $\delta p_c^{break} > \delta p_c^{clog}$.However, we show in Farge et al. (2021) (Section 4.1) that

because both tortuosity and pore aperture change when pores open, the change of permeability is more important than the ratio of the δp threshold, which only depend on pore aperture, therefore $k_{hi}/k_{lo} > \delta p_c^{break}/\delta p_c^{clog}$ and $q_c^{break} < q_c^{clog}$. In this case, values of flux determine three distinct valve behaviors:

- When $q_{in} < q_c^{break}$, the flux is lower than the breaking threshold, and valves will stay closed, or close if they are open.
- When $q_{in} > q_c^{clog}$, the flux is higher than the closing threshold, and valves will stay open, or open if they are closed.
- When $q_c^{break} < q_{in} < q_c^{clog}$, a closed valve will open because $q_{in} > q_c^{break}$, and as $q_{in} < q_c^{clog}$, the now-open valve will eventually close. In these conditions, valves are permanently unsteady, opening and closing in cycles, generating sustained activity.

In experiments with model porous media, the permeability state (clogged, unclogged or variable) undergoes similar phase transitions depending on the fluid input rate in the system (Jäger et al., 2017; Bianchi et al., 2018).

Figure 3 upper panels (a–f) display the cycle of pressure and permeability for a valve, for three values of q_{in} in the range allowing sustained activity $q_c^{break} < q_{in} < q_c^{clog}$. The closer the input flux q_{in} is to either threshold values, the closer the valve will be to a permanently closed or open state, as seen in the time series of valve permeability (Figure 3b, d, f). For instance in Figure 3a, the flux is just above q_c^{break}. After a rapid increase of δp when the valve closes, the closed valve is close to an equilibrium and it lets fluid seep through it as the flux loads it, at a barely superior rate. δp will relatively slowly reach the breaking threshold δp_c^{break}. When the valve eventually opens, the background flux is so low that δp quickly drops to the closing point δp_c^{clog}. Overall, the valve spends most of the time closed, close to opening conditions for q_{in} just above q_c^{break}. Conversely, if q_{in} is higher, just below q_c^{clog}, the valve takes a much longer time to close when open, and opens very quickly when closed: it spends more time open overall.

This behavior is reflected in the time averaged properties of the valve cycle as a function of flux, displayed in Figure 3g and h. When close to threshold, the valve rarely switches states, and produces few events — openings. When q_{in} is far from the critical values, the valve rapidly loads and relaxes. Because the cycle is faster, the activity rate is higher. Finally, the proportion of the time the valve is open smoothly transitions from a mostly closed state to a mostly open state from q_c^{break} to q_c^{clog}, matching the static regime beyond those values. This progressive permeability evolution from a clogged to an unclogged state for increasing values of the hydraulic stressing rate has been observed in injection experiments in the lab (Candela et al., 2014).

Two other parameters shape the valve cycle: valve width w_v and the ratio of closed to open permeability $\lambda = k_{hi}/k_{lo}$. Valve width governs how quickly fluid can sip through the valve, and how strong the fluid flux near a valve has to be to impose a given δp across it. We will show that as two valves of width w_v are close enough, they start behaving as a macro-valve of larger width. Therefore, the width w_v should be considered the elementary width at which the heterogeneity of permeability is defined, but other scales of heterogeneity will emerge in systems of many valves where spatial cluster of valves behave as macro-valves, and we fix $w_v = 0.01$ for all valves in the rest of the study. As permeability is the only transport property that is variable in space, the value of λ describes how quickly fluid pressure diffuses inside a valve relative to outside of it in the high permeability channel. When this ratio is very high, diffusion within the valve is much slower than outside the valve, and the effects of the pressure variations outside the valve will thus dominate the dynamics. In this study, we take $\lambda = k_{hi}/k_{lo} = 20$, for which closed valves virtually behave as barriers to the fluid diffusion, and the exact value of this ratio essentially does not influence valve dynamics. Our final goal being to under-

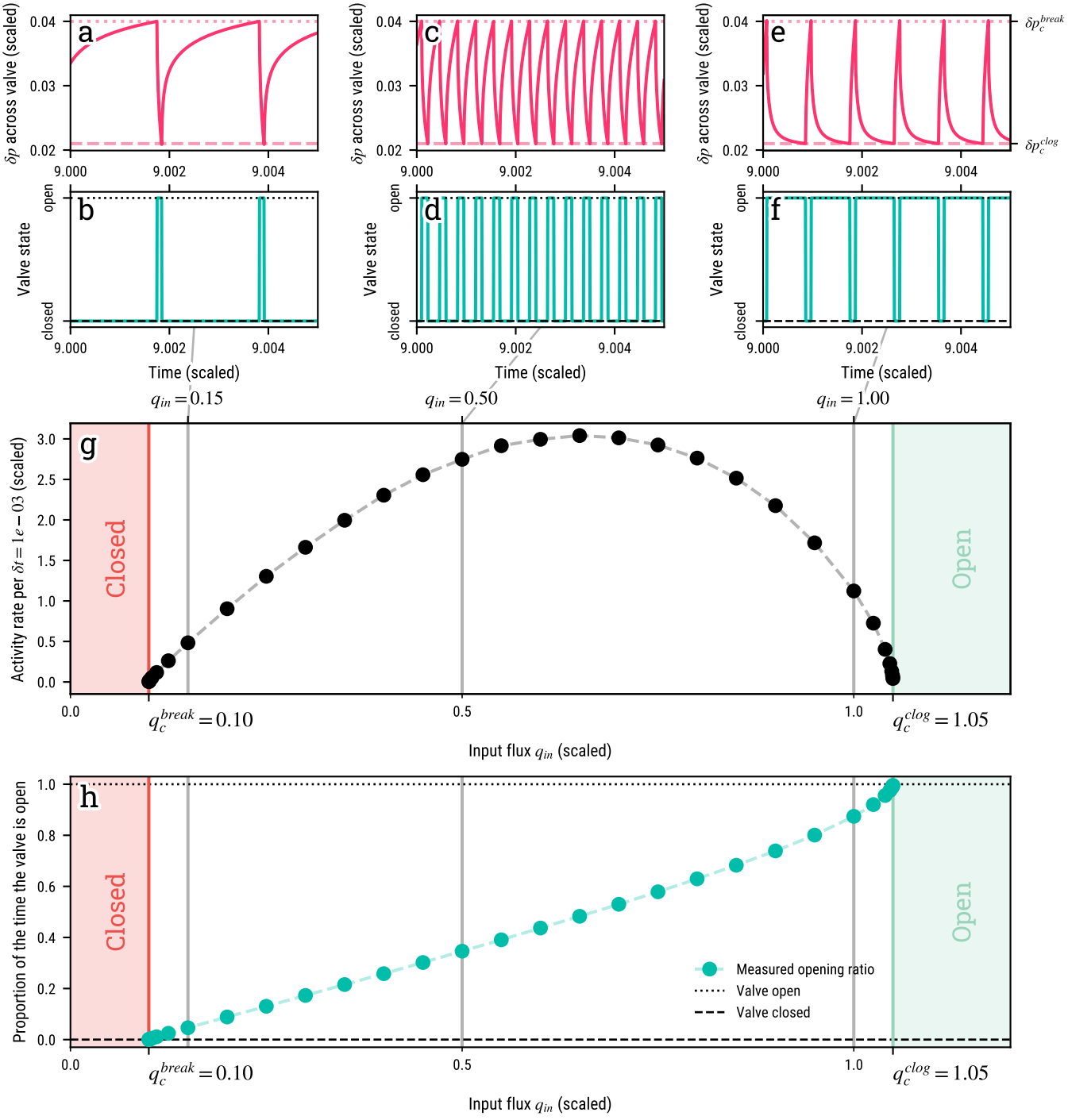

Figure 3. Temporal behavior of a single valve, subjected to different values of the input flux q_{in}, within the range allowing sustained valve activity, $q_c^{break} < q_{in} < q_c^{clog}$. The upper panels *(a), (c), (e)* display the temporal evolution of fluid pressure difference δp across the valve, while panels *(b), (d), (f)* show the state of the valve in time, for the same three values of the input flux. See text for a detailed explanation of the regime at each value of q_{in}. *(g)* Rate of valve openings — model seismic events and *(h)* proportion of the time a valve is open as a function of q_{in}. In both *(g), (h)*, the activity rate and opening ratio are measured when the behavior of the valve has reached a steady state. For low (resp. high) q_{in}, the valve is closer to threshold, and spends more time in a closed (resp. open) state, close to threshold. Further away from the critical values

Table 1. Valve parameters for all simulations presented in this study

	Parameter	Value (scaled)
w_v	Valve width	0.01
k_{hi}	Open valve permeability	1
k_{lo}	Closed valve permeability	0.05
δp_c^{break}	Threshold p difference for opening	0.02
δp_c^{clog}	Threshold p difference for closing	0.0105
q_c^{break}	Flux above which a closed valve will open	0.1
q_c^{clog}	Flux below which an open valve will close	1.05

stand how large-scale, complex patterns of valve activation emerge from interactions between elementary valves, all valves in the rest of the study have fixed parameters (Table 1). The main control parameters on valve activity will therefore be the value of the input flux q_{in} relative to the opening and closing thresholds, and the valve distribution — their number N_v and position relative to one another in the channel.

4 Characterizing source interaction in a two-valve system

4.1 Valves interact through pressure transients

In order to understand how valves interact through pressure transients and which parameters control how strong and fast this interaction is, we first design systems with two valves, and observe how they evolve. Valves are at equal distance from the center of the channel $x = 0.5$ in normalized length units. The valve width is $w_v = 0.01$, and the distance between them is d_v, normalized to w_v (Figure 4a).

In Figure 4, we describe a simulation in which a system with two valves at a distance of $d_v = 0.8w_v$ is subjected to a low flux $q_{in} = 0.13$ — close to q_c^{break}, the critical flux above which closed valves will open. In the permanent regime and independently of the initial conditions, we observe that the cycles of pressurization and release of both valves (Figure 4b) eventually synchronize, with a short, consistent delay between the first valve's opening (downdip valve) and the second valve's opening (updip valve). The valves open and close synchronously, and events associated with each opening therefore occur in a two-event burst, recurring every valve cycle.

As we zoom in on the last opening sequence of the simulation (Figure 4c), we observe that the updip valve is affected with a short delay by the downdip valve's opening and the flux pulse that it produces. δp across the closed updip valve suddenly rises due to the fluid influx behind it, and as it is already close to failure, it is sufficient to bring it to open. It should be noted that in Farge et al. (2021) Section 4.2, we have shown that this triggering interaction does not necessarily occur from the downdip valve towards the updip valve. Indeed, the effect of a valve opening updip creates a transiently low pressure in front of the downdip valve, that can trigger its opening.

The triggering interaction between valves is therefore carried by the fluid pressure field in the permeable system. Because it is a diffusive system, the further the triggering pressure transient has to travel to the neighboring valve, the more the interaction between the valves is damped and slow. In other words, the distance between valves d_v should be an essential control on the interaction strength and synchronization.

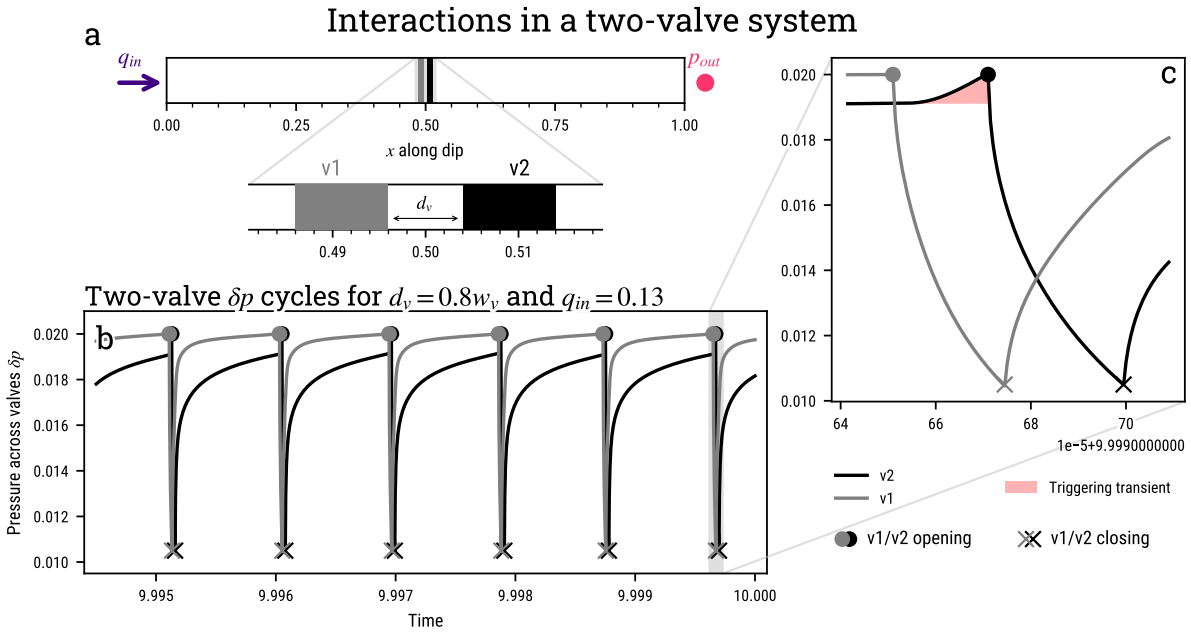

Figure 4. Interactions in a two-valve system. *(a)* A system with two valves (v1 and v2) spaced by $d_v = 0.008 = 0.8w_v$, subjected to a constant flux $q_{in} = 0.13$, and a constant pressure output $p_{out} = 0$. *(b)* Cycles of fluid pressure accumulation and release are shown with the time-series of the pressure difference δp across v1 and v2. Closing and opening occur when δp reaches a pre-defined threshold. *(c)* As v1 opens first and when v2 is critically stressed, the pressure transient that its opening produces (in red) triggers the opening of v2, after a short delay.

The sensitivity of valves to small variations of pressure around them is also directly related to their *criticality*: their being close or far to the threshold of δp that will make them change state — open or close. As shown in the previous section and Figure 3, the amount of time δp at the valve spends close to threshold is controlled by the value of the input flux q_{in}. The closer q_{in} is to critical values q_c^{break} or q_c^{clog}, the closer to thresholds the valves are on average. In Figure 4b and c, the input flux is $q_{in} = 0.13 \approx q_c^{break} = 0.1$ and it is visible that both v1 and v2 approach δp_c^{break} tangentially. Thus, the closer q_{in} is to critical values, the stronger the interactions between two valves should be, as the smallest change of pressure is likely to trigger opening of the valve when it is closed, and closing of the valve when it is open.

4.2 Valve spacing controls activity synchronization

In order to characterize the influence of the intervalve distance d_v on the synchronization of valve activity, we design two-valve systems with various d_v, spanning $d_v = 0$ to $20w_v$. All systems are subjected to a constant flux, and we characterize the event recurrence timescales when the permanent regime is reached. Various values of flux are tested for all systems, and in Figure 5, we display the results of this experiment for three domains of q_{in}, and for the full range of intervalve distances.

As the two valves are identical, during the permanent regime of all simulations, the events occur in repeated sequences of alternating events: a two-event burst (Figure 5). Two timescales therefore characterize the activity:

- δt_{intra} the time interval between the first and second opening of the burst

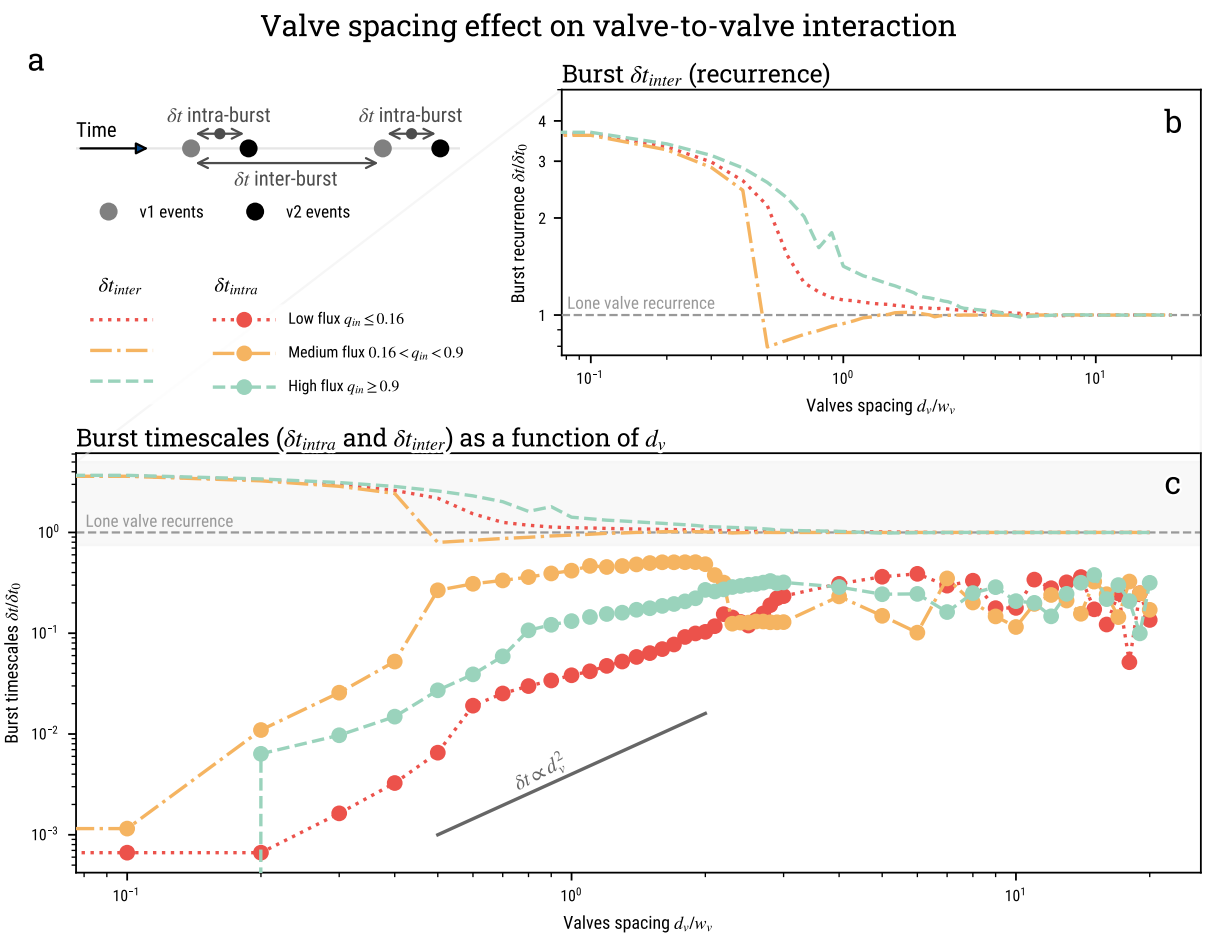

Figure 5. Effect of valve spacing on valve-to-valve interaction. *(a)* Two timescales describe a two-event burst: δt_{intra} is the delay between events in the burst, and δt_{inter} is the recurrence delay of the burst. In *(b)* and *(c)*, we observe how δt_{inter} (no markers on the line) and δt_{intra} (circle markers) evolve as a function of valve spacing for low (red, dotted line), intermediate (yellow, dash-dot line) and high (green, dashed line) flux values. Both timescales are normalized by δt_0, the period of activation of a valve subjected to the same flux. For sufficiently large valve spacing ($d_v > 5w_v$), valves do not interact and act as isolated valves. As valves get closer, events get closer, and the bursts are less frequent.

- δt_{inter} the time interval in between the beginnings of two neighboring bursts, which can be thought of as the burst recurrence time.

In Figure 5b and c, we show the evolution of these two timescales, normalized by δt_0 the period of the cycle of an isolated, identical valve subjected to the same flux.

The first observation is that at large distances ($d_v > 5w_v$, Figure 5b), bursts — therefore events for each valves — occur with a recurrence corresponding to an isolated valve: the cycle of either valve is not affected by the other valve.When the distance between the valves gets shorter, the interaction between valves becomes stronger, producing two effects on the valves' cycle. *(1)* In Figure 5c, we observe that for all fluxes, the closer the valves are (the lower d_v), the shorter δt_{intra} is. As valves get closer, the events

are closer in time, and valves synchronize. *(2)* In Figure 5b, we observe that as valves get very close ($d_v < 0.5w_v$ for $q_{in} = 0.11$), δt_{inter} increases for lower and lower d_v — for all three domains of flux. In other words, the closer the valves, the longer the recurrence delay between bursts, and the less frequently valves activate. For such close proximity between valves, the inter-event time is so short that the two valves together can be considered as a twice-wider *macro-valve*. Interestingly, in Figure 5, we see that for all fluxes, the *macro-valve* consistently activates with about 4 times the delay of an isolated, elementary valve. We reported the emergence of similar macro-valving behavior in systems of many strongly-interacting valves in our previous study (Farge et al., 2021, Section 5.3).

A comparison of the curves corresponding to the low, medium and high input flux ranges in Figure 5b and c allows to assess the effect of the q_{in} on the interaction strength. In Figure 5b, we see that for low and high q_{in} ranges (red and green curves), which are closer to critical opening and closing thresholds, the deviation of δt_{inter} from the reference cycle period (grey line) happens for valve spacings that are wider than for the medium flux range (yellow curve). Indeed, when subjected to a medium flux range, valves are further away from criticality most of the time, and they have to be closer neighbors to interact with a similar intensity as when they are more critical. The same observation can be made for the delay between events in bursts δt_{intra}: shorter valve spacings are necessary in the medium flux range to reach a similarly short delay between events in bursts, compared to the high and low, closer to criticality, flux ranges.

Here, we have demonstrated that the interaction between two identical valves are stronger when *(1)* they are closer together, *(2)* the flux q_{in} they are submitted is close to the thresholds of opening or closing, putting them in a near-critical state. As interactions get stronger, the valves synchronize in time, and their behavior starts resembling that of a larger, less active macro-valve, with different effective permeability and triggering thresholds.

5 Emergence and variability of synchronization in complex valve systems

5.1 Control parameters and simulation setup

In reality, the complex permeability of a fault-zone channel should be composed of many heterogeneously distributed valves. In such systems, the synchronization of sources is more complex, and could rely on intricate hydraulic interactions. Based on the results for the two-valve experiments, we investigate how the input flux in the system and the valve distribution shape interactions in complex N_v-valve systems, and are conducive to intermittent, clustered activity, and quasi-perfect periodicity of bursts. To do so, we run simulations in complex channels with many identical valves, systematically testing how the valve distribution along-dip and values of q_{in} relative to the opening and closing thresholds (q_c^{break}, q_c^{clog}) affect the modeled tremor activity.

In the previous section, we have shown that the distance between two valves d_v controls the strength of interactions for a given input flux. In a system with $N_v >> 1$ valves, the low-permeability segments can be close together either because there are many of them in the system, or because of their spatial clustering which results in dense patches separated by less populated regions. In order to test the effect of density and spatial clustering of valves, we design systems where the low-permeability barriers are distributed using a Weibull distribution for the inter-valve distance d_v. The probability density function of the distribution is:

$$p(d_v) = \frac{u}{d_0}\left(\frac{d_v}{d_0}\right)^{u-1} \times \exp\left((-d_v/d_0)^u\right), \tag{7}$$

and its mean

$$\overline{d_v} = d_0 \Gamma \left(1 + \frac{1}{u}\right). \tag{8}$$

where d_0 is the scale parameter, u the shape parameter of the distribution, and Γ is the gamma function.

The Weibull distribution provides a straightforward parameterization of valve density and spatial clustering in the system, allowing to choose between perfectly regular and highly clustered distributions solely with the choice of the shape parameter u in equation 7. Indeed, when $u \to +\infty$, the distribution tends toward a Dirac in d_0 — valves are regularly spaced, at a distance of $d_v = d_0$. When $u \to 0$, the Weibull distribution tends to a power law distribution $p(d_v) \propto d_v^{-1}$. In this case, most valves are spaced with very small d_v, and rarely, a large spacing is drawn, producing a clustered valve distribution. Finally, for $u = 1$, the Weibull distribution reduces to an exponential distribution $p(d_v) = \exp(-d_v/d_0)/d_0$, of mean $\overline{d_v} = d_0$. In this case, the number of valves in a segment of given length follows a Poisson distribution, and valves are more or less homogeneously distributed across the channel, although at random. As a rule of thumb, this distribution produces clustered point distributions for $u < 1$, and more homogeneous and regular valve distributions for $u \geq 1$. Finally, the choice of d_0 will allow to specify the average valve distance $\overline{d_v}$, and therefore number of valves N_v in the system (equation 8).

A valve system is built by first specifying a buffer zone on each sides of the system to reduce edge effects, common for all distributions, then by randomly drawing inter-valve distances using the chosen parameters (u and $\overline{d_v}$), and finally distributing them on the regular space grid, by simply rounding down the inter-valve distance to the closest discrete distance possible. We also ensure that the spacing of the last valve to the one before that is not too far from the target inter-valve distance, so that all valves do not end up near the input for the most clustered valve distributions. Figure 6 describes the density-clustering (N_v–u) space of distributions available to us using this technique. Figures S7 and Figures S8 in the Supplementary Information file give a more complete illustration of this distribution space.

We run more than 42,000 simulations, for distributions described by $N_v = 9$–71 ($\overline{d_v} = 9.5w_v$–$0.2w_v$, 16 values), $u = 0.2$–9 (8 values, 128 theoretical distributions in total). We randomly generate 30 distributions for each (N_v, u), in order to average out the effects of specific valve arrangements on our results, and obtain statistical significance. In all systems, valves have identical width, closed permeability and opening/closing δp thresholds (Table 1). Each system thus defined (3840 total) is subjected to different values of input flux $q_{in} = 0.11$–1.04 (11 values), with denser sampling close to the thresholds allowing valve opening ($q_c^{break} = 0.1$) and closing ($q_c^{clog} = 1.05$). In all valve simulations, the output pressure is kept at $p_{out} = 0$.

In addition to pressure, flux and permeability in time and space, we record valve states in time and space, and build a catalog of valve activations to simulated a seismicity for each simulation. This catalog is then automatically characterized by computing:

- the activity rate, measured by the average event count per valve in a given time increment δt,
- the extent to which activity occurs in clusters with the clustering index c ($c = 0$ events are not clustered at all, $c = 1$ all events occur within clusters),
- the recurrence timescales of clusters in cases when the activity is clustered in time ($c > 0.25$), measured as the average delay $\text{mean}_k(\Delta T_k)$ between clusters of a same size,
- and how stable in time the recurrence is, using as an indicator the ratio of the average to the standard deviation of the measured delays $\text{mean}_k(\Delta T_k)/\text{std}_k(\Delta T_k)$. When $\text{mean}_k(\Delta T_k)/\text{std}_k(\Delta T_k) > 2$, a simulation is labelled "periodic".

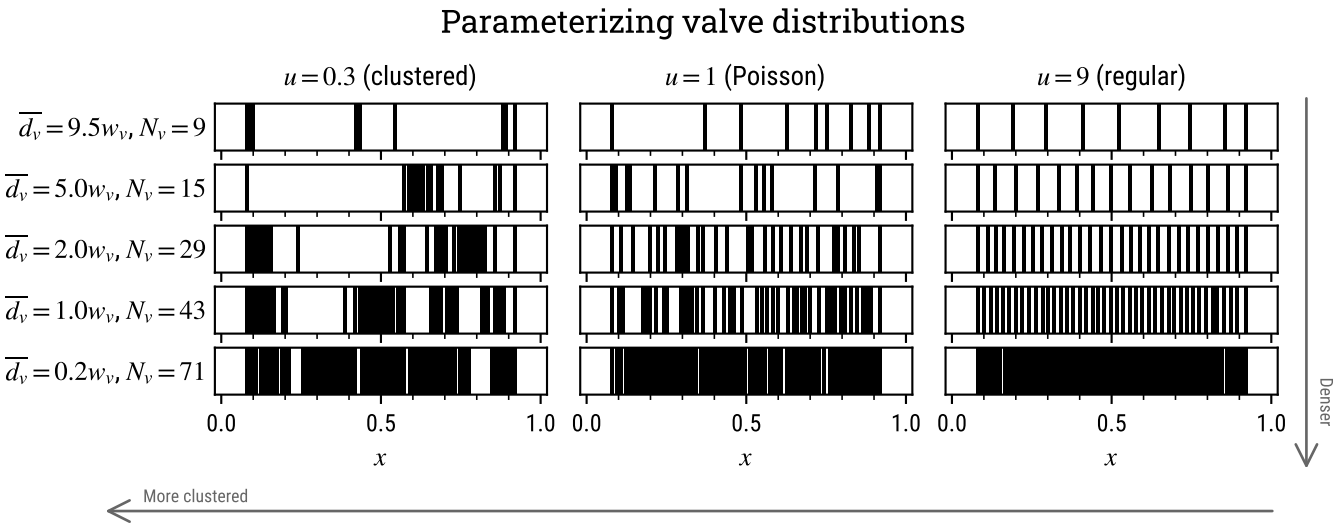

Figure 6. Valve distributions are generated by drawing valve distances d_v using a Weibull distribution. The valve density, or average valve distance in the domain $\overline{d_v}$, and therefore the number of valves in the system, are controlled by the theoretical mean of the distribution. The shape parameter u of the Weibull distribution allows to control how clustered or regularly-spaced valves are in space.

The details of how the latter three measures are computed can be found in Section 2.3.

5.2 Control of the input flux on activity synchronization

In the previous sections we showed that when the input flux q_{in} is close to the thresholds of opening (q_c^{break}) and closing (q_c^{clog}), valves are more sensitive to small changes of pressure. In Section 4, we show that this results in strong interactions between valves in two-valve systems subjected to near-threshold q_{in}. With stronger interactions, valve activity tends to synchronize, producing less frequent, more synchronous bursts of events. In Farge et al. (2021), we demonstrated that near-threshold fluxes produce a more clustered seismicity in valve systems with $N_v = 29$ valves, with $u = 1$ (Poissonian valve distribution). Here, we will generalize this analysis to the full spectrum of densities and spatial clustering of valves.

We start by focusing on the activity produced in a clustered valve system, $u = 0.3$, with $N_v = 29$ valves ($\overline{d_v} = 2w_v$), for three values of the flux: *(a)* $q_{in} = 0.13$, near the opening threshold of valves q_c^{break}, valves are mostly closed in average (Farge et al., 2021), *(b)* $q_{in} = 0.57$, far from thresholds, *(c)* $q_{in} = 1.02$ near the closing threshold of valves q_c^{clog}. Figure 7 displays the results of the experiment. The first observation is that the results from the two-valve system generalize to this system with $N_v > 2$. In *(a)* and *(c)*, q_{in} is close to threshold, and activity is intermittent, organized in clusters of events in time, which recur quasi-periodically, whereas when q_{in} is far from threshold (in *(b)*), activity is more continuous, and less clustered. In this system at least, the input flux controls the synchronization of valve activity: the closer to threshold it is, the more clustered and periodic the activity seems to be. A second observation is that coherent pat-

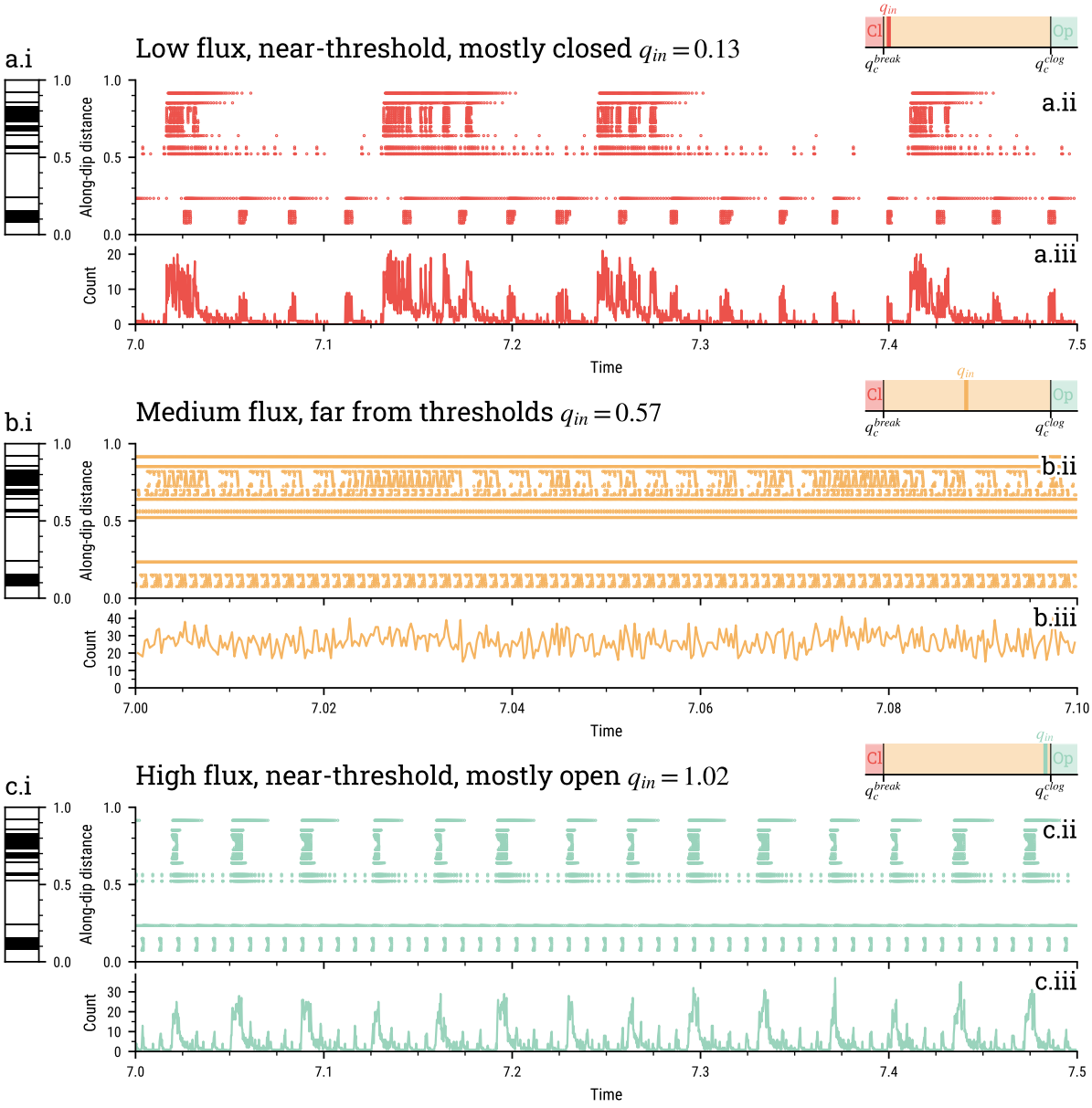

Figure 7. Synthetic tremor activity for three values of the input flux q_{in} (a, b, c) in the same, clustered valve system ($u = 0.3$, $N_v = 29$, $\overline{d_v} = 2w_v$, system b in Figure 9). Panels *(a.i)*, *(b.i)* and *(c.i)* represent the valve distributions along the channel. Panels *(a.ii)*, *(b.ii)* and *(c.ii)* display the activity along the channel in time, in a time-space diagram where each dot represents the location and time of an opening event. Panels *(a.iii)*, *(b.iii)* and *(c.iii)* show the event count (per bin of $\delta t = 2.5e-4$) time series. The colored panels represent a flux scale, on which q_{in} is represented relative to the opening and closing thresholds. The closer to threshold q_{in} is, the more valves are sensitive to interactions, as they spend more times in a given state. This produces a more synchronized, clustered activity, recurring on long periods. The reader should note the dilated time scale in simulation *(b)*.

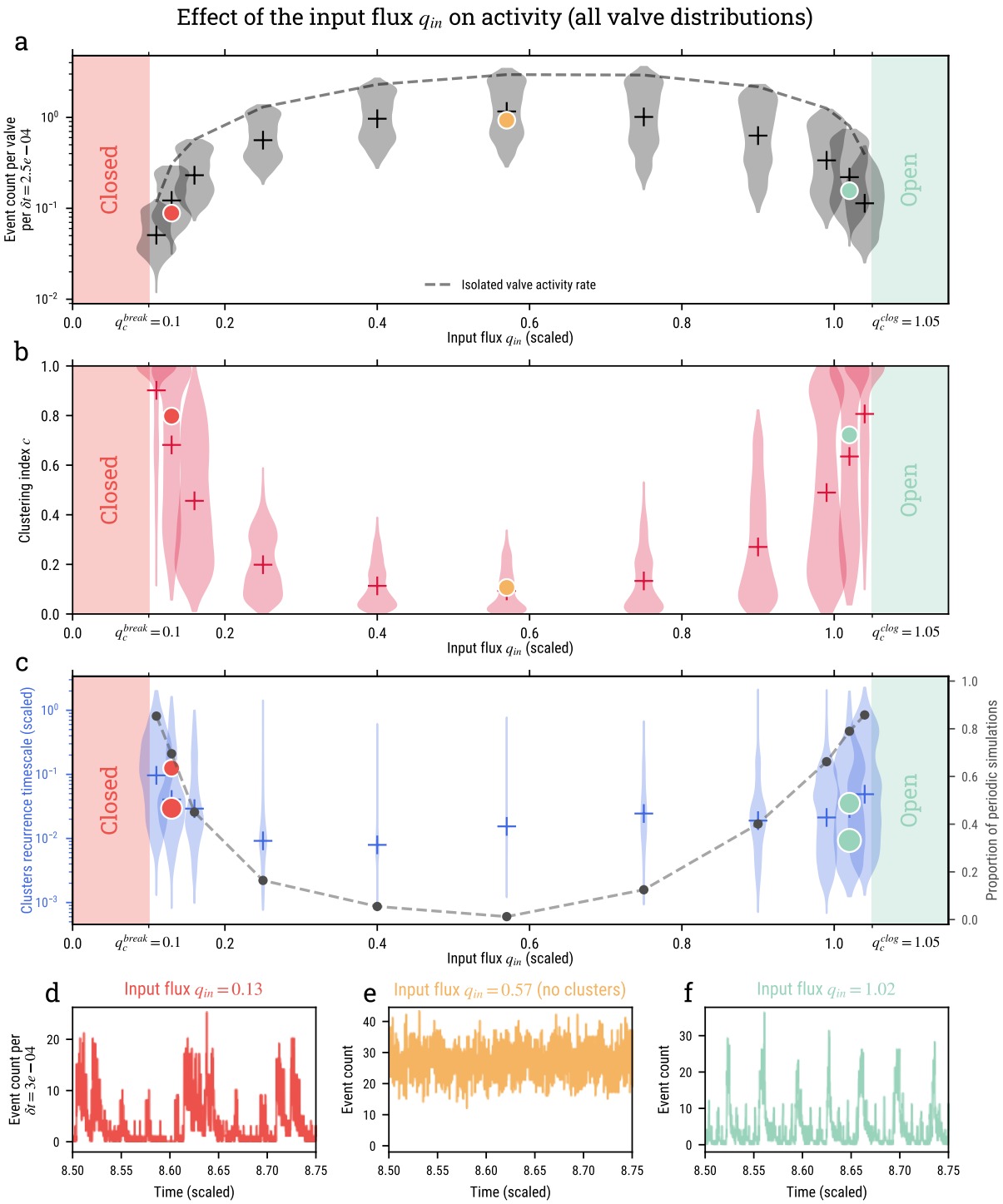

Figure 8 Caption on next page.

Figure 8. Activity rate, temporal clustering and recurrence timescales for different values of the input flux q_{in}, for all valve distributions. *(a)* Activity rate, computed as the number of events per valve per $\delta t = 2.5e-4$ (scaled time units). *(b)* Level of activity clustering measured with the clustering index c, for different values of q_{in}. *(c)* The average recurrence delay for clusters, as a function of q_{in}. The grey dotted line represents the proportion of periodic simulations (see text for explanation) for each value of q_{in}. In panels *(a)*, *(b)* and *(c)*, the distribution of measured values for each value of q_{in} is visualized with a violin plot, and the median of all measurements for this q_{in} is represented as a cross. The domains where the flux value prohibits valve activity are shown with red (all valves closed) and green (all valves closed) patches. The colored dots show the clustering and recurrence for the activity in a given system, subjected to three values the input flux. Each corresponding time series of activity is displayed in the bottom panels *(d)*, *(e)* and *(f)*. The three simulations are performed on a clustered valve distribution ($u = 0.3$) with $N_v = 29$ valves ($\overline{d_v} = 2w_v$), system b displayed in Figures 9b and 11e.

terns of activity build over larger distances when the flux is closer to threshold. Indeed, when q_{in} is far from threshold, activity is intermittent, but it synchronizes on a much smaller spatial scale than when q_{in} is near-threshold. When valves are more critical, triggering interactions can cascade farther in the system, as most valves are in the same state: close to threshold, and therefore sensitive to the opening or closing of their neighbor. When the flux is farther from threshold, valves cannot synchronize as well in time and space, as there is less chance that the pressure transient when a valve opens will reach a near-threshold valve. As in a two-valve system, the long-range interaction allowed by near-critical fluxes allows large-scale, long-period cycles of activity for large clusters of valves ($0.5 < x < 1$ in Figure 7a.ii). As valves synchronize in space and time, a large-scale valving behavior emerges, favored by valve criticality.

Using the full range of our simulations, we extend the analysis to all valve systems, to observe how they respond to values of the flux in between the closing and opening thresholds. Figure 8 synthesizes our results. For all valves systems, dense or sparse, clustered or regular, the closer q_{in} is to critical values of the flux, the closer valve systems are to staying closed ($q_{in} \approx q_c^{break}$) or open ($q_{in} \approx q_c^{clog}$). In Figure 8a, we see that valves therefore produce less events just as a result of flux conditions, but also because of valve-to-valve interactions. Interactions between neighboring valves force them into a less frequent activation (Figure 5). The closer q_{in} is to thresholds, the more synchronized the activity gets. Valve activity synchronizes in clusters ($c > 0.5$), and long-range interactions produce macro-valving behavior, which tends to make the activity more periodic, and with longer periods (Figure 8b and c). As in real systems, periods of burst recurrence ($T \sim 10^{-2}$–1) are orders of magnitude longer than the period of individual valve cycles ($T \sim 10^{-4}$–10^{-3}). When valves in the system witness a flux that is further from critical conditions, they open and close rapidly, without time to interact and build synchronicity: activity is high, less clustered, less periodic, with shorter periods.

In subduction zones (*e.g.* in Shikoku, Figure 1), most regions exhibit strong temporal clustering ($c > 0.7$), timescales of burst recurrence several orders of magnitude longer than individual source recurrence, and coherent activity in space, over scales larger than the individual source scale. Such conditions are only found in our system for input fluxes into the fault zone that are near-threshold, both low and high. However, it seems unlikely that the permeable system in the fault zone could stay mostly open. Because of the high temperature and pressure, ductile deformation of pores and crystallization processes in the pores would rapidly shut most of the pathways (Tarling et al., 2021), and form pockets of fluid, separated by low-permeability barriers (Gold & Soter,

1985). The near-threshold, low-flux regime ($q_c^{break} < q_{in} < 0.3$) therefore seems to be the more realistic part of the flux domain. According to our model, in real subduction zones, a small decrease in flux (between spatial regions or in time) could therefore result in a monotonic decrease in seismicity, and favor interactions between permeability valves, thus further lowering seismicity rates, and producing a more clustered, more periodic activity, synchronizing over larger distances and longer periods. For the rest of this study, we will thus focus our analysis on low, near-opening-threshold values of the input flux, $q_{in} < 0.3$.

5.3 Control of the valve distribution on activity synchronization

In Section 4.2, we showed using a simplified system that the interaction between two valves gets stronger and faster as the distance between them decreases. Those effects should persist in a more complex system: the closer the valves get in the system, the more synchronized in time and long-period the activity should be. In order to independently demonstrate the effect of an increase in valve density ($\overline{d_v}$ and N_v) and spatial clustering (u), we use the activity in three valve systems, *(a)* a rather homogeneous system, with $N_v = 29$ valves ($\overline{d_v} = 2w_v$) and a Poissonian distribution of valves ($u = 1$), *(b)* a system with the same valve density ($N_v = 29$, $\overline{d_v} = 2w_v$) but a more clustered valve distribution $u = 0.3$, and finally *(c)* a denser system ($N_v = 43$, $\overline{d_v} = 1w_v$), with the same spatial clustering as in the previous system ($u = 0.3$). All three valve systems are subjected to a low input flux $q_{in} = 0.13 \approx q_c^{break}$. Figure 9 summarizes the results.

System *(a)* produces temporally-clustered activity, occurring in bursts, with however less variability than the other two systems. Indeed, System *(b)* (Figure 9b.i, b.ii, b.iii) shares the same number of valves and average valve spacing as System *(a)* however the higher spatial clustering of valves creates dense patches of valves in the system, where valves are locally much closer together than the average inter-valve distance d_v. The resulting activity is more synchronized, it proceeds in clearly separated bursts — of two sizes, in two different regions of the domain. The burst recurrence is quite variable, but is obviously longer than for bursts produced in System *(a)*. Finally, System *(c)* (Figure 9c.i, c.ii, c.iii) is as spatially clustered as System *(b)*, but with more valves. It is the system where on average valves are the closest, and also with the most places where valves are very close locally. The activity it produces is the most clustered of the three: it proceeds in bursts of two sizes, almost without any activity otherwise. They occur almost periodically, with a more constant, longer period than System *(b)*. Strikingly, the overall activity rate in System *(c)* is lower than in the other two: as noticed in a two-valve system, the longer-recurrence intervals of activity episodes decrease the activity rate of valves in the system.

The level of synchronicity of activity increases both as spatial clustering u increases (*(a)* to *(b)*) and as valve density increases (*(b)* to *(c)*). This shows that as valves get closer in the system, their interactions generate stronger interactions, which build clusters of activations. As elementary valves form spatial clusters in the channel, their collective behavior builds macro-valves, which produce the bursts of activity seen in system *(b)* for instance ($x \approx 0.1$ and $x > 0.5$). The most striking result here is that even though valve clusters in the channel are far apart, the collective effect of a macro-valve on the pressure field is such that it builds long-range interaction between valve clusters, which synchronize valve clusters throughout the channel. This effect occurs in system *(c)*, where a large-scale valving behavior emerges at the scale of the whole channel, as the four valve clusters synchronize their activity. In a previous study, we have shown that such cycles of activity are associated with cycles of permeability opening and closing, fluid pressure accumulation and release, similar to the cycle of a single valve (Farge et al., 2021). The different scales of macro-valving allowed by interactions — cluster of valves (system *(t)*, $x < 0.2$), cluster of valve clusters (system *(t)*, full channel) — build increasingly long

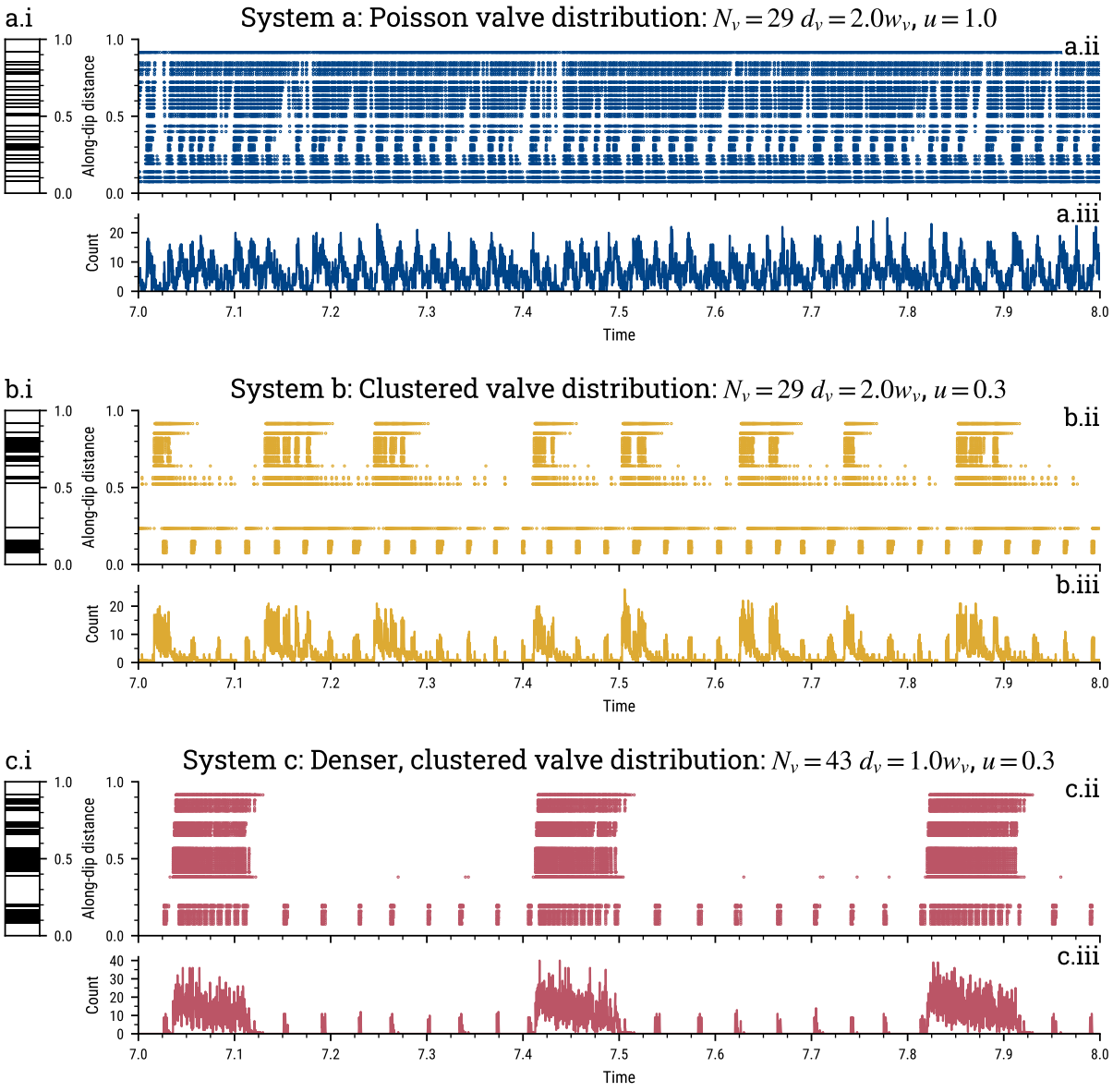

Figure 9. Synthetic tremor activity for three valve systems with different density and clustering (*a*, *b*, *c*). Panels *(a.i)*, *(b.i)* and *(c.i)* represent the valve distributions along the channel. Panels *(a.ii)*, *(b.ii)* and *(c.ii)* display the activity along the channel in time, in a time-space diagram where each dot represents the location and time of an opening event. Panels *(a.iii)*, *(b.iii)* and *(c.iii)* show event count (per bin of $\delta t = 2.5e-4$) time series. The denser and more clustered the valve system, the more clustered and periodic the activity, and the longer the timescales of recurrence. In other words, the closer the valves get in the system, the more synchronized and long-period the resulting activity seems to become.

periodicity of activity, as fluid has to diffuse from the input throughout the closed system to load all valves to the point of breaking before a collective reopening of the system.

This test is therefore consistent with our hypothesis. The closer the valves get, either due to spatial clustering (lower u) or more numerous valves (higher N_v, lower $\overline{d_v}$), the more synchronized their activity is: they all activate at the same time during bursts, and are inactive outside of those episodes. In addition, the activity seems to also display longer recurrence timescales as the valves are closer locally in the system.

A simple measure of how many valves are interacting in the system N_v^{int} should capture how u and N_v both affect the intermittence of activity, and conveniently reduce the dimension of the problem. We define N_v^{int} as the number of valves that have a neighbor closer than $0.5w_v$, on either side. The value of $d_v < 0.5w_v$ as an interacting distance is chosen on the basis of the the two-valve experiments described in Section 4: in Figure 5c, it is visible that valves interact very strongly at distances lower than $d_v = 1w_v$ and that this effect is even clearer for $d_v > 0.5w_v$. We choose the lower bound, $d_v < 0.5w_v$ for the interacting distance. When the activity characteristics are plotted along N_v^{int}, we capture the effects of the local proximity of valves in the system, either due to spatial clustering or overall density. Figure 10 shows systems with different N_v^{int}, showing that a similar number of valves can be at interaction distance when the system is dense and not very clustered, and when it is less dense but with stronger spatially clustered valves.

The results outlined in the previous paragraphs stand for all valve distributions. In Figure 11, the activity rate, temporal clustering and periodicity are plotted as a function of the number of interacting valves N_v^{int}, for all valve distributions, subjected to a low value of flux, close to the closing threshold $q_{in} = 0.13$. The three simulations from 9 are shown as colored dots in panels a, b, and c, and represented again in d, e and f. The

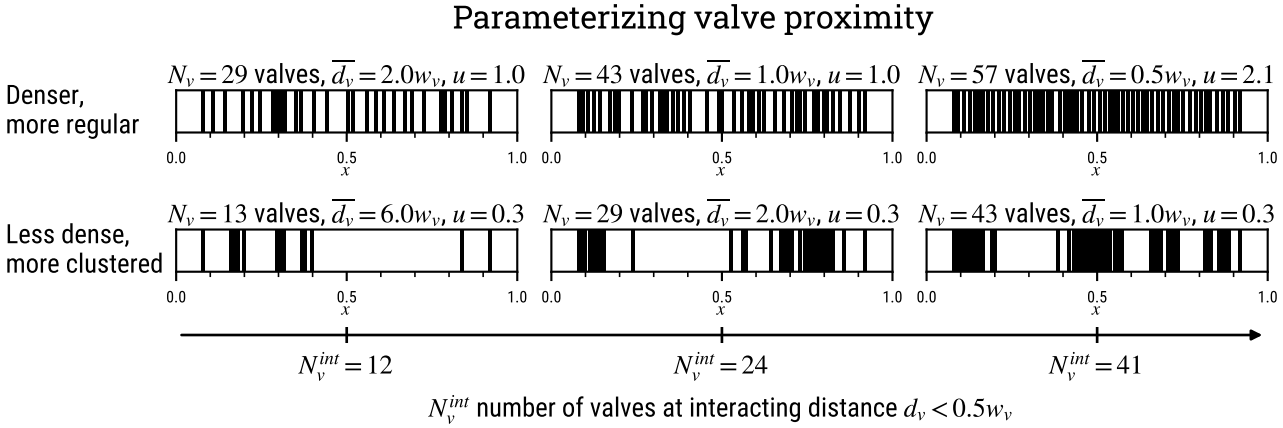

Figure 10. The number of interacting valves N_v^{int} is a measure of how much valves are close from each other in a valve system, either owing to the density of the system (N_v, $\overline{d_v}$), or to the spatial clustering (u). As valves get closer, they interact more, and N_v^{int} seems to be the best parameter to capture the effects on the style of activity.

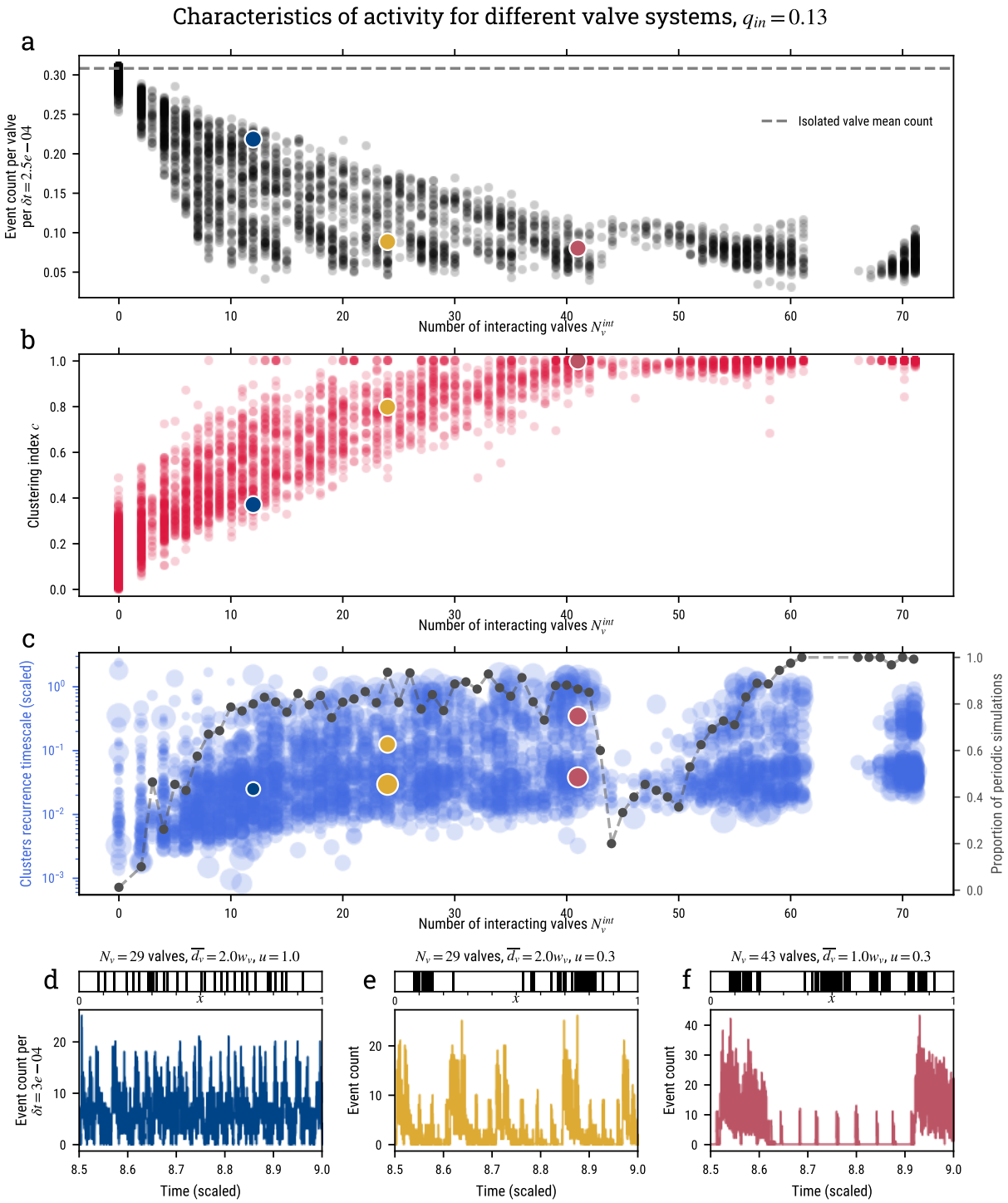

Figure 11: Caption on next page

Figure 11. Intensity, clustering and recurrence timescales of activity for varying levels of interaction in complex valve systems. Results for $q_{in} = 0.13$. *(a)* Average event count per valve according to the number of interacting valves N_v^{int}. *(b)* Level of activity clustering measured with the clustering index c, as a function of N_v^{int}. *(c)* Timescales of cluster recurrence as a function of N_v^{int}. The detected timescales are represented as dots which size scales with the variability of the measured recurrence, estimated as the ratio of the average to the standard deviation of the inter-cluster delays, in the given simulation. The transparency of each data dot is used to convey the density of points in the graph. The dotted line represents the proportion of periodic simulations (see Section 2.3 for details) for each value of N_v^{int}. In panels *(a)*, *(b)* and *(c)*, the circled, colored dots show the values of clustering and recurrence for three valve systems with increasingly strong valve interactions (same $q_{in} = 0.13$). The three bottom panels *(d)*, *(e)* and *(f)* show the corresponding valve distributions (top) and activity (bottom).

signature of increasing interactions in the system is visible as the number of valves at interacting distance rises in the system, due to both more clustered or denser distribution. The closer valves get in the system, the stronger their interactions, and the more clustered their activity gets ($c > 0.5$, Figure 11b). As they interact strongly, they form macro-valves, and their activity rate drops (Figure 11a), they activate in clusters with a more and more periodic behavior (Figure 11c). Finally, as more and larger clusters form with increasing density and spatial clustering of valves, the activity synchronizes on larger distances, and becomes periodic on longer timescales (Figure 11c). Strikingly, the various space scales of synchronization (macro-valves) seem to be reflected in the detected periodicities of activity: both short- ($T \approx 3 \times 10^{-2}$) and long-period ($T \approx 3 \times 10^{-1}$) are detected, corresponding roughly to periodicities of small valve clusters (of width ~ 0.2), and of the full channel — *e.g.* system *(c)* in Figure 9. Once more, it is noteworthy that the periods of activity bursts ($5{\times}10^{-3}$ to 1 scaled time units for most detected periods) that emerge are orders of magnitude longer than the period of an isolated valve cycle (8.1×10^{-4} scaled time units for an isolated valve with $q_{in} = 0.13$).

The noticeable drop in number of periodic simulations for $N_v^{int} = 45$–50 is an artifact due to the way we design valve systems. In order to test perfectly regular valve systems, the tested values for N_v jump from 43 to 57. As $N_v^{int} \leq N_v$, systems with $N_v^{int} = 45$–50 are systems which degree of spatial valve clustering is low ($u > 1$), putting valves far apart. In this case, valve clusters in space are few and small, which results and a less periodic activity, and lower periodicities — when they emerge.

6 Discussion

6.1 Linking model parameters and subduction zone hydraulic properties

The spatio-temporal patterns of intermittence of tremor in subduction zones gives the most direct access to minute deformation and hydraulic processes occurring within or around the subduction interface (*e.g.* Bernaudin & Gueydan, 2018; Cruz-Atienza et al., 2018; Luo & Liu, 2019). In this work, we propose a simple representation of the hydraulic processes in the fault based on elementary permeability-valve processes, in order to investigate the role that hydraulic dynamics may play in shaping the intermittence of tremor. The main characteristics of tremor we seek to reproduce and understand are the emergence of the strong temporal clustering of events (Idehara et al., 2014; Frank et al., 2016; Poiata, Vilotte, Shapiro, Supino, & Obara, 2021), the long, quasi-periodic recurrence of tremor bursts (Brudzinski & Allen, 2007; Frank et al., 2014; Husker et al.,

2019; Poiata, Vilotte, Shapiro, Supino, & Obara, 2021), and how of those two phenomena vary along the strike of tremor source regions in subduction zones, at scales of tens to hundreds of kilometers (Brudzinski & Allen, 2007; Poiata, Vilotte, Shapiro, Supino, & Obara, 2021). The model we developed reproduces such patterns of seismicity because of interactions between elementary seismic sources, through fluid pressure transients in the permeable fault interface. We showed that these interactions are the basis of the emergence of time and space scales of coherent activity much wider than the time and space scale of activation of a single, isolated source. This feature of our results is valid for a wide range of the control parameters in our system, and it therefore seems that large-scale, spatio-temporal patterns of LFE activity in reality could be influenced by slow hydraulic interaction between sources. In the system we describe, interactions are controlled by the criticality of valves (q_{in} *vs* valve thresholds) and valve distribution.

We argue that in reality valves should spend most of their times closed, and the input flux be above, but near their opening threshold q_c^{break}, producing highly intermittent, on-off activity (*cf* Section 5.2). In our system, the distance between q_{in} and q_c^{break} controls the intermittence of activity. It can change due to changes of *(1)* q_{in}, *(2)* of valve breaking threshold δp_c^{break}, and finally *(3)* of the permeability of the valve when closed k_{lo}. More generally, those parameters represent *(1)* an hydraulic stressing rate, *(2)* an hydraulic weakness (or strength), and *(3)* how much it translates flow into stress, a kind of stress-leakage term. The segmentation of tremor intermittence in a real subduction zone could therefore rely on spatial variations of those parameters. The variations of fluid input is due in part to spatial variations in focusing of the flow in large-scale permeable channels (Piccoli et al., 2021; Eymold et al., 2021; Angiboust et al., 2014; Ague, 2014), perhaps dug by past subduction of seamounts (Ide, 2010). The thickness of the subducting crust, speed and angle of the subduction also controls dehydration rate (Maury et al., 2018). Variations in temperature can affect how well the fault interface is sealed from above by silica deposits (Audet & Bürgmann, 2014), and therefore the importance of sinks and leaking along the fault-zone, which competes with loading rate, inhibiting valve activity (*e.g.* Halpaap et al., 2019). Finally, the intrinsic properties of the fault zone govern the strength and permeability of valves, and can strongly be affected by the geology of the subducting and overriding plates, and local level of damage, controlling both the availability of pathways for the fluid to circulate and the plasticity of the fault zone material. Other studies have suggested that local increase in flux and availability of high fluid pressures might increase the frequency of tremor bursts (McLellan et al., 2022; Wech & Creager, 2011), but our work stresses that the intensity of q_{in} has to be compared to the relative contribution of strength and sinks in fluid pressure accumulation in the fault zone.

Indeed, the emergence of temporal clustering and large time and space scales of tremor activity also relies on the number of interacting sources, which in our description is directly based on the permeability structure of the fault zone. Our results tend to show that long-range synchronization and longer timescales are built through the collective behavior of dense patches of permeability valves in the channel (Section 5.3). Macro-valves built out these patches have a strong effect on the pressure field. They are wide, mostly closed segments of the permeable channel in the fault zone, and by opening all at once, they generate strong, long-period, long-wavelength variations of fluid pressure, which can diffuse farther than the transients generated by elementary valve openings, and therefore can synchronize the valving and seismic activity of wide parts of the fault zone. In Section 5.3, we show that for more than $N_v^{int} = 20$ valves at interacting distance, the produced seismicity is highly temporally clustered, quasi-periodic, on timescales orders of magnitude longer than single-valve cycles. For the valve widths used here $w_v = 0.01$, this corresponds to at least 20 % of the system behaving in a valve-like manner, with significant spatial clustering of those elementary segments. If it were the case, the observed patterns of tremor activity could be driven by large-scale, long-period fluid pressure and permeability transients in the fault zone, built on elementary valving processes. In other

words, N_v^{int} is a rough description of the heterogeneity of permeability of the fault zone. It is linked with the amount of larger scale irregularities of permeability, which end up behaving as macro-valves. Ridges, seamounts or fracture zones dominate the kilometric roughness of the subduction plane, and should define macro structures of permeability in the fault. Such structures generate kilometric-scale heterogeneities of stress, damage, permeability, and mechanical properties of the fault zone. As tremor sources seem to also be spatially clustered in patches (Rubin & Armbruster, 2013; Ide, 2010; Chestler & Creager, 2017), the spatially-clustered Weibull distribution ($u < 1$) seems to reasonably approximate the physical and observational characteristics of the tremor zone.

6.2 Plate topography and tremor segmentation in Shikoku

Long-wavelength geophysical observations in subduction zones, of magnetic or gravimetric anomalies for instance, reveal that subduction zones are structurally segmented on a scale of tens to a hundred of kilometers. This segmentation seems to emerge mostly from the topographic and internal structure of the subducting oceanic plate (Blakely et al., 2005; Wannamaker et al., 2014; K. Wang & Bilek, 2014; Shillington et al., 2015; Bassett & Watts, 2015), which displays heterogeneous structures — ridges, seamounts, fracture zones — on such a scale. As rough terrain enters the subduction, it modifies stress, damages both the subducting and overriding plate, carries more sediments and water into the subduction. Those factors can directly affect how seismicity manifests in the rough segment by modifying the mechanical properties of the fault zone. And indeed, the structural heterogeneity of the subducting plate often correlates with the spatial variations of seismicity and tremor along strike in subduction zones, on a very similar scale as the observed topographic features of the incoming seafloor (Blakely et al., 2005; K. Wang & Bilek, 2014; Shillington et al., 2015; Bassett & Watts, 2015; Ide, 2010). The topography of the incoming plate could directly affect the permeability structure, valving properties and channeling of the fluid in the fault zone. In the next paragraph, we use the results of our model to try to link the segmentation of activity in Shikoku with geologic-scale properties of the plate interface, and interpret how the topography of the subducting Philippine Sea plate could be the underlying cause of these spatial variations.

In Section 2 (Figure 1), we used our novel characterization techniques to propose a kilometric-scale segmentation of tremor intermittence in Shikoku. Three segments can be identified: the first two segments (segment 1 and 2) at each along-strike extremity ($d < 140$ km, and $d > 190$ km, Figure 1, Figure 12), are characterized by a high level of clustering and relatively short timescales of recurrence ($T \approx 3$ months). Segment 3 in between is characterized by low, almost exclusively clustered activity, with a longer, clearer period ($T \approx 6$ months). Interestingly, Ide and Yabe (2014) show that the dominant focal mechanism of very-low-frequency earthquakes (VLFEs) are different between each of those region — a segmentation that our model cannot account for. In Figure 12, we see that the along-strike extent of those segments and spots of high tremor activity within them is quite similar to the dimension of seamounts on the seafloor of the Philippine plate, or the ones observed in the accretionary wedge (Yamazaki & Okamura, 1989): about a few tens of kilometers. The alignment of the Kinan seamount chain with the segmented tremor zone along the convergence direction could indicate that such structures on the subducting slab, or their lasting effects on the medium as they plow at depth, are the main factor shaping the segmentation of activity in the Shikoku tremor zone.

The segmentation of tremor intermittence in Shikoku can be interpreted as contrasts of activity synchronization in time and space, and therefore of interaction strength between sources. Stronger or weaker source-to-source interactions produce more (segment 3) or less (segments 1 and 2) clustered, periodic activity, with more or less coherence on large scales of time and space. Our work goes beyond this general interpretation by showing that such interactions can occur in a dynamically permeable channel

in the fault zone, and that the criticality of sources and their spatial distribution directly control the interaction strength, and therefore shape the intermittence of activity.

The input flux q_{in} partly controls how close valves are to threshold, and therefore how triggerable they are. If valves are relatively similar for the three segments in Shikoku, the lower activity, higher temporal clustering and clearer-defined, longer periodicity in the buffer segment (segment 3, 140 km $< d <$ 190 km along-strike) can be due to a relatively lower metamorphic flux in the region compared to the neighboring regions 1 and 2. The locally lower q_{in} would impose a slower build up of pressure behind the permeability valves, which would spend more time in a closed state, close to their opening threshold. Segment 3 would therefore produce a lower seismicity, and a more clustered, long-period activity than the end segments 1 and 2, as valves would be closer to threshold. The same criticality contrast between segments can also arise from a difference in valve strength, assuming the input fluid flow — and transport properties of the channels — does not vary significantly along-strike. The valves in the buffer, segment 3, could indeed be stronger — higher breaking threshold and/or lower permeability — but undergoing the same fluid input rate. For a constant input flux along-strike, this results in the same variation of criticality along strike: valves in the buffer region are closer to threshold, producing a more clustered and long-period activity, and valves in the segments 1 and 2 framing it are further from threshold, producing a less clustered, more intense and shorter-period activity. Both these effects can stem from the presence of, or lasting effects of one or several subducting seamounts (Ide, 2010), that strongly fracture the medium in the end segments of the tremor zone. The amount of fluid that comes through the interface around the tremor source region would be enhanced by a channeling effect, and simply by a higher volume of dehydrating crust at depth. In Figure 12, the alignment of the Kinan seamount chain with the subducting seamount detected by Yamazaki and Okamura (1989) and the tremor zone could indicate that the chain extends into the subduction, and could result in the tremor activity patterns observed there. Segment 3 that produces lower, longer-recurrence activity can be a smoother, less damaged region, in which less fluid is channeled because of a lower channeling effect, and a lower overall permeability. In this case, the low flux create a longer recurrence time of periods of opening and activity. Although it might explain the observed activity patterns and it seems like the most direct interpretation of the intermittence of a system of hydraulic pressure accumulation and release (McLellan et al., 2022), this interpretation might be at odds with observations of tidal and dynamic triggering on tremor in patches of highest activity in the end segments of the zone, and not in the buffer zone (Miyazawa et al., 2008; Chao et al., 2013; Chao & Obara, 2016; Kurihara et al., 2018). Indeed, if seismicity in the segments is triggered by minute strains on the interface, it suggests that those segments might actually be closer to criticality: valves would be more sensitive to the very small δp changes across them generated by the dynamic strains of tides and teleseismic waves.

It therefore seems that the segmentation could arise from spatial variations of permeability structure, caused by large-scale heterogeneity in the subducting plate topography. In a first order analysis, we can assume that the input flux in fault channels, the background transport properties and the permeability valve characteristics do not significantly change across the strike of the tremor zone. A contrast of valve density and clustering in each segment would therefore explain the segmentation of intermittence. In this interpretation, we can explain the characteristic activity in the buffer zone, segment 3, as being due to a higher level of interaction between valves, for instance coming from a higher valve density in this region compared to the neighboring ones. In geological terms, this would mean a lower overall permeability in segment 3, but a larger share of the system being dynamic. This could be due to a more homogeneous permeable system, perhaps because of a relatively smooth segment of oceanic plate being subducted in this region. A dense, highly interacting valve network, would produce a remarkably synchronized and periodic activity in both time and space and lower overall activ-

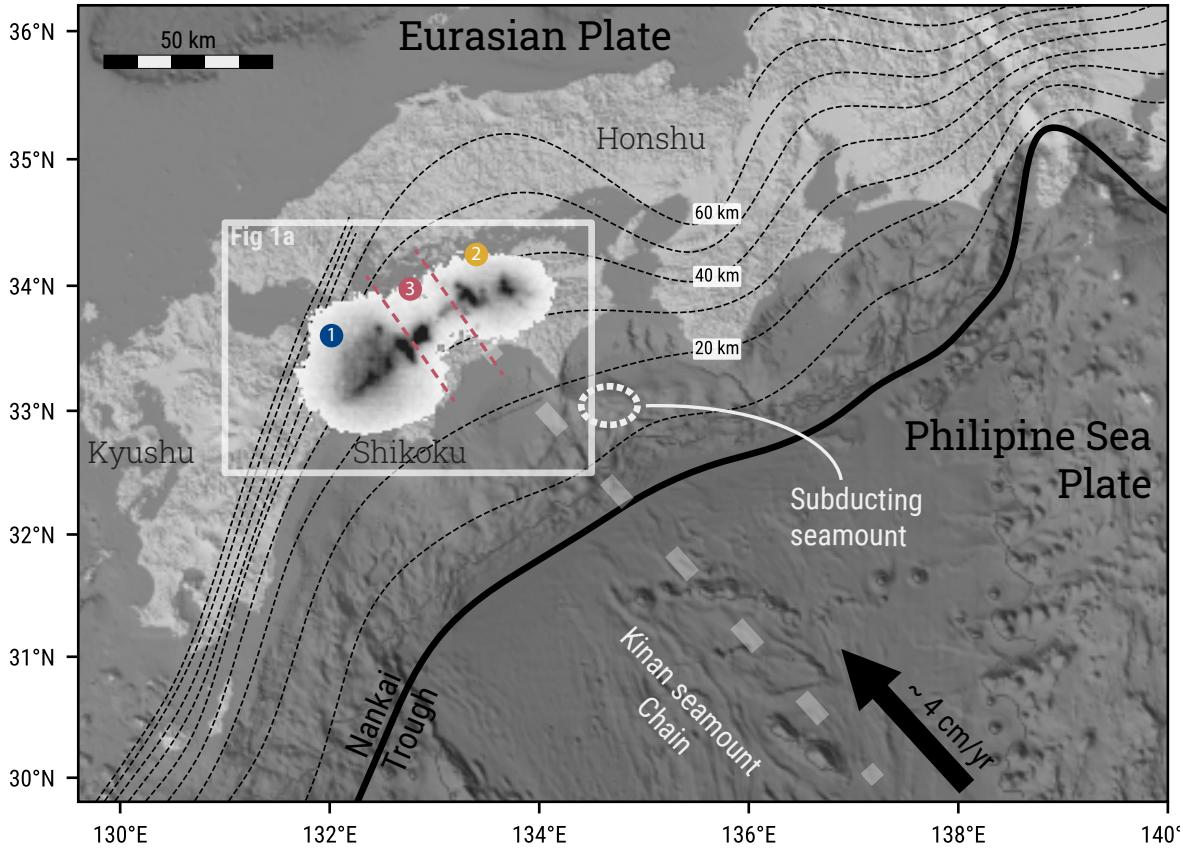

Figure 12. Regional context of the Shikoku subduction and tremor zone. The trench is outlined in thick black line, and the depth contours of the slab are shown in thin dotted black line (model from Iwasaki et al. (2015)). The black arrow and wide dotted line show the direction of relative convergence of the Philippine plate, towards the Eurasian plate (fixed). The extent of the map in Figure 1a is shown with the white box. The three segments defined using the activity are indicated by the numbered circles and dotted lines that divide the tremor zone. We single out rough topographic features on the subducting Philippine plate: the Kinan seamount chain, and a subducting seamount (Yamazaki & Okamura, 1989). Because of their alignment with the tremor zone, and their consistent spatial scale, the presence such topographic features could be responsible for the segmentation of activity witnessed in Shikoku, and displayed as a 2D histogram on the map (*cf* Figure 1 for details).

ity rate (Figure 9c and 11), and seems that it well describes the seismicity in segment 3. In this interpretation, the high valve density in the buffer zone would behave as a subduction-scale valve for the pressure circulation along-strike.

6.3 Scope and limitations of model geometry

In the previous section, we used our results on space-averaged intermittence of activity in along-dip channels as representative of the activity in wide segments along the

strike of the subduction. This approach assumes that the behavior of each segment can be explained by along-dip dynamics of fluid pressure, and that it is isolated from its neighbors, as we neglect the connectivity along-strike. As tremor zones often extend far wider along-strike than along-dip (*e.g.* Cascadia and Nankai), and as tremor exhibit migrations of activity along-strike, and finally, as hydraulic and solid stresses should propagate in all directions, our approach simplifies the problem greatly.

However, we argue that the dynamics in the segments we defined in Shikoku can reasonably be collapsed along-dip for our analysis. Indeed, along-strike migrations within segments do not require significant flow nor strong fluid pressure gradients along-strike. Indeed, the fluid source, coming from a band of dehydrating slab around 80 km depth, applies a hydraulic stress in the updip direction, in the form of a strong gradient of fluid pressure. If tremor indicates permeability opening, its migrations along-strike indicate the propagation of a pulse of acceleration of updip flux, releasing the updip gradient of pressure. In this case, the difference between the direction of fluid pressure gradient and the direction of propagation of the opening of permeability is similar to that of stress and rupture propagation for a mode III crack.

In order to explore this set-up, the model could be extended as a network of parallel, along-dip channels, connected along-strike — through smaller channels or valves, for instance. As valves open in one of the channels, the transients of pressure could be communicated along-strike, and trigger the opening of valves in neighboring channels, thus simulating along-strike propagations of seismicity. We can speculate that this might reproduce the observation that tremor activity progresses along-strike accompanied by rapid sweeps along-dip, in the principal permeability channels (Ghosh et al., 2010). The model would then essentially depend on a competition between along-strike and along-dip connectivities, which dictates the preferential direction of propagation of pressure transients, and therefore tremor activity. This could explain why the buffer zone seems to act as a barrier to large migrations of seismicity in the neighboring segments: it opens and lets pressure transients circulate through more rarely and regularly, only when a large enough pressure difference along-dip has built up across it, depending on its past activity mainly.

6.4 Interactions between fluid circulation and fault slip

The larger question our work aims to ask is: is fluid pressure and permeability driving the dynamics of tremor activity or is fault slip. This model does not intend to faithfully reproduce spatiotemporal patterns of tremor activity, or fluid pressure variations in the subduction interface. It is however a framework to reflect about the role of hydraulic stress dynamics with more spatial and temporal complexity. By only looking at the dynamics of the hydraulic system, we show that it can reproduce characteristic behavior of tremor and fluid pressure in the fault zone, and that spatial variations of hydraulic properties can lead to variations in tremor intermittence, therefore providing a mechanism that could shape the observed along-strike segmentation of tremor.

It however clear to us that slip should be implicated in generating tremor and that the spatial variations of its dynamics play a role in the segmentation of tremor (Nakajima & Hasegawa, 2016; Kano et al., 2018; Cattania & Segall, 2021). Fault slip and tremor activity are linked because their occurrences are to some degree correlated in space and time (*e.g.* Rogers, 2003; Hall et al., 2019). At the same time, this correlation is not perfect and detailed observations that the slow slip and tremors are not perfectly co-located on the same fault segments (*e.g.* Kostoglodov et al., 2010). Nevertheless, the tremor activity can be used to detect the geodetic signature of small slow slip transients otherwise buried in the noise (Frank, Radiguet, et al., 2015). In this interpretation, the tremor is generated as brittle asperities rupture when a slip transient occurs on the subduction fault (Ando et al., 2010). The seismic characteristics of LFEs — their radiation pattern

mostly — are also consistent with shear slip on the subduction interface (Ide et al., 2007; Royer & Bostock, 2014), although observations interpreted that way are sometimes ambiguous, and could sometime fit a single-force mechanism as well (Wech & Creager, 2007; Shapiro et al., 2018; Ohmi & Obara, 2002). The spatio-temporal patterns of tremor would therefore be shaped by the dynamics of slip in conditions of near-lithostatic fluid pressure and heterogeneity of frictional properties of the fault interface (*e.g.* Wech & Creager, 2011; Sweet et al., 2019; Luo & Liu, 2019).

The processes of unclogging — or hydrofracture of low permeability barriers — and transient fluid pressure that we describe should interact closely with slip on the fault. As slip occurs on the fault, be it seismically or aseismically, it generates an extensional regime in parts of the fault zone, allowing extension veins to open and pump fluid into the fault (Kotowski & Behr, 2019), thus strongly modifying the local permeability and fluid pressure in the slipping region. Damage and dilatancy in and around slip also create permeability (Tenthorey & Cox, 2006; Mitchell & Faulkner, 2008; Im et al., 2019), and can therefore also affect the fluid pressure field.

On the other hand, it is known that high fluid pressure can trigger slip on a fault by lowering the fault strength. The most plausible cause of an increase of fluid pressure is an input of fluid in a partly sealed region. In a homogeneous channel, such fluid flow is necessarily associated with a smooth pressure gradient, implying that the high fluid pressures that are required for sliding motion are limited to the neighborhood of the source. Our study shows how heterogeneous and transient permeability behavior in the fault could generate high fluid pressures locally and transiently, in wide parts of the subduction zone. The collective behavior of valves creates a cumulative effect on fluid pressure that translate into multi-scale fluid pressure increases and drops, that could shape the behavior of fault slip from the source to the subduction scale, thus shaping tremor activity, as hinted by the geological record (Angiboust et al., 2015; Taetz et al., 2018; Muñoz-Montecinos et al., 2021; Tarling et al., 2021).

We believe the next step in our approach is to understand what scales and observable behaviors of tremor activity, fluid pressure or slip are specific to a fluid-dominated or a deformation-dominated regime, and therefore can help distinguish between both in the field. To do so, experimental, theoretical and modeling work is needed to better describe the coupling between deformation (induced by pressure and/or slip) and permeability, and what physical parameters control which regime the system is in.

7 Conclusion

The present work should be understood as a simple framework emphasizing the role of fluid pressure transients in the occurrence of tectonic tremor in subduction zones. Our study is based on the premise that clustering and quasi-periodicity of seismic activity should occur when sources synchronize, through interactions. As they synchronize, the activity of numerous sources becomes coherent over large scales of space and time. In order to measure as explicitly as possible the synchronization of sources, we build novel and simple measures of temporal clustering and periodicity in a point-process description of tremor activity. We propose that the interactions at the origin of the observed intermittency of tremor may be mediated by fluid pressure transients in the permeable fault zone. In our description, elementary tremor events (LFEs) occur when permeability valves open within the fault zone, stressed by the incoming metamorphic fluid flux channeled in the fault zone. We find that how close valves are to their activation threshold — resulting from a competition between the intensity of the fluid pressure source and their mechanical strength — and their spatial distribution in the fault zone both control the intermittency of their collective behavior.

In our framework, the highly-clustered, long-period activity of the buffer segment in the Shikoku tremor zone develops when densely-packed, highly-interacting valves activate collectively, thus building subduction-scale valving behavior accompanied by large bursts of activity. The large timescales of activity, and remarkable spatial coherence of the tremor bursts thus emerge from small-scale fluid pressure and permeability cycling in the dynamic fault zone, building up through interactions between dynamic segments. The segmentation of activity in the tremor zone seems directly linked with the topography of the subducting Philippine Sea plate. While the rough terrains in the extremity of the tremor zone should favor less critical valves and a rougher, sparser distribution of valves, the smoothness of the slab surface in the buffer segment produces a dynamics adequately represented by a dense valve system. Our model therefore provides a simple, physically-based mechanism to describe the influence of hydrological processes on shaping tremor patterns in both space and time. More work is needed to refine the physical description of hydromechanical processes in this framework, in particular the interplay between the slip, the fluid pressure and the permeability. However, we argue that including dynamic hydrological processes is crucial to understand tremor and microseismicity patterns in general. Beyond the subduction zone setting, we therefore expect the permeability-valve framework has a broader reach to interpret how unsteady fluid circulation processes shape the dynamics of a wide range of geologic plumbing systems (Journeau et al., 2022; Wech et al., 2020; Ross et al., 2020; Gosselin et al., 2020; Materna et al., 2019).

Open Research Section

The catalogs of tremor and LFE used in this study are available at `https://doi.org/10.31905/UOQ9LVHZ` for Shikoku, Japan (Poiata, Vilotte, Shapiro, Supino, & Obara, 2021; Poiata, Vilotte, Shapiro, Obara, & Supino, 2021), in the supporting information of Husker et al. (2019) for Guerrero and Oaxaca (Mexico), and at `https://pnsn.org/tremor` for Cascadia (Wech & Creager, 2008). The code — still in active development — for the model is available at `https://github.com/gfarge/PPvalves`.

Acknowledgments

This study was supported by the European Research Council under the European Union Horizon 2020 research and innovation program (Grant Agreement 787399-SEISMAZE). Numerical computations were performed on the S-CAPAD/DANTE platform, IPGP, France. The authors thank S. Rondenay, E. Brodsky, C. Cattania, A. Schubnel, K. Chanard, two anonymous reviewers and the editor for constructive discussion that led to significant improvement of this manuscript.

References

Ague, J. J. (2014, January). 4.6 - Fluid Flow in the Deep Crust. In H. D. Holland & K. K. Turekian (Eds.), *Treatise on Geochemistry (Second Edition)* (pp. 203–247). Oxford: Elsevier. doi: 10.1016/B978-0-08-095975-7.00306-5

Anderson, R. N., Uyeda, S., & Miyashiro, A. (1976, February). Geophysical and Geochemical Constraints at Converging Plate Boundaries–Part I: Dehydration in the Downgoing Slab. *Geophysical Journal International*, *44*(2), 333–357. doi: 10.1111/j.1365-246X.1976.tb03660.x

Ando, R., Nakata, R., & Hori, T. (2010). A slip pulse model with fault heterogeneity for low-frequency earthquakes and tremor along plate interfaces. *Geophysical Research Letters*, *37*(10). doi: 10.1029/2010GL043056

Angiboust, S., Kirsch, J., Oncken, O., Glodny, J., Monié, P., & Rybacki, E. (2015, June). Probing the transition between seismically coupled and decoupled segments along an ancient subduction interface. *Geochemistry, Geophysics, Geosystems*, *16*(6), 1905–1922. doi: 10.1002/2015GC005776

Angiboust, S., Pettke, T., De Hoog, J. C. M., Caron, B., & Oncken, O. (2014, May). Channelized Fluid Flow and Eclogite-facies Metasomatism along the Subduction Shear Zone. *Journal of Petrology*, *55*(5), 883–916. doi: 10.1093/petrology/egu010

Audet, P., & Bürgmann, R. (2014, June). Possible control of subduction zone slow-earthquake periodicity by silica enrichment. *Nature*, *510*(7505), 389–392. doi: 10.1038/nature13391

Audet, P., & Kim, Y. (2016, February). Teleseismic constraints on the geological environment of deep episodic slow earthquakes in subduction zone forearcs: A review. *Tectonophysics*, *670*, 1–15. doi: 10.1016/j.tecto.2016.01.005

Bassett, D., & Watts, A. B. (2015, May). Gravity anomalies, crustal structure, and seismicity at subduction zones: 1. Seafloor roughness and subducting relief: CRUSTAL STRUCTURE AND SEISMICITY: 1. SUBDUCTING RELIEF. *Geochemistry, Geophysics, Geosystems*, *16*(5), 1508–1540. doi: 10.1002/2014GC005684

Beaucé, E., Frank, W. B., Paul, A., Campillo, M., & Hilst, R. D. (2019, November). Systematic Detection of Clustered Seismicity Beneath the Southwestern Alps. *Journal of Geophysical Research: Solid Earth*, *124*(11), 11531–11548. doi: 10.1029/2019JB018110

Beaucé, E., van der Hilst, R. D., & Campillo, M. (2022, September). Microseismic Constraints on the Mechanical State of the North Anatolian Fault Zone 13 Years After the 1999 M7.4 Izmit Earthquake. *Journal of Geophysical Research: Solid Earth*, *127*(9). doi: 10.1029/2022JB024416

Behr, W. M., & Bürgmann, R. (2021, March). What's down there? The structures, materials and environment of deep-seated slow slip and tremor. *Philosophical Transactions of the Royal Society A: Mathematical, Physical and Engineering Sciences*, *379*(2193), 20200218. doi: 10.1098/rsta.2020.0218

Ben-Zion, Y. (2012, May). Episodic tremor and slip on a frictional interface with critical zero weakening in elastic solid: NVT-ETS and criticality. *Geophysical Journal International*, *189*(2), 1159–1168. doi: 10.1111/j.1365-246X.2012.05422.x

Bernaudin, M., & Gueydan, F. (2018, April). Episodic Tremor and Slip Explained by Fluid-Enhanced Microfracturing and Sealing. *Geophysical Research Letters*, *45*(8), 3471–3480. doi: 10.1029/2018GL077586

Bianchi, F., Thielmann, M., de Arcangelis, L., & Herrmann, H. J. (2018, January). Critical Bursts in Filtration. *Physical Review Letters*, *120*(3), 034503. doi: 10.1103/PhysRevLett.120.034503

Blakely, R. J., Brocher, T. M., & Wells, R. E. (2005). Subduction-zone magnetic anomalies and implications for hydrated forearc mantle. *Geology*, *33*(6), 445. doi: 10.1130/G21447.1

Bostock, M. G., Thomas, A. M., Savard, G., Chuang, L., & Rubin, A. M. (2015). Magnitudes and moment-duration scaling of low-frequency earthquakes beneath southern Vancouver Island. *Journal of Geophysical Research: Solid Earth*, *120*(9), 6329–6350. doi: 10.1002/2015JB012195

Brudzinski, M. R., & Allen, R. M. (2007). Segmentation in episodic tremor and slip all along Cascadia. *Geology*, *35*(10), 907. doi: 10.1130/G23740A.1

Brudzinski, M. R., Hinojosa-Prieto, H. R., Schlanser, K. M., Cabral-Cano, E., Arciniega-Ceballos, A., Diaz-Molina, O., & DeMets, C. (2010, August). Nonvolcanic tremor along the Oaxaca segment of the Middle America subduction zone. *Journal of Geophysical Research*, *115*, B00A23. doi: 10.1029/2008JB006061

Calvert, A. J., Preston, L. A., & Farahbod, A. M. (2011, August). Sedimentary underplating at the Cascadia mantle-wedge corner revealed by seismic imaging. *Nature Geoscience*, *4*(8), 545–548. doi: 10.1038/ngeo1195

Candela, T., Brodsky, E. E., Marone, C., & Elsworth, D. (2014, April). Laboratory evidence for particle mobilization as a mechanism for permeability enhancement via dynamic stressing. *Earth and Planetary Science Letters*, *392*, 279–291. doi: 10.1016/j.epsl.2014.02.025

Cattania, C., & Segall, P. (2021, April). Precursory Slow Slip and Foreshocks on Rough Faults. *Journal of Geophysical Research: Solid Earth*, *126*(4). doi: 10.1029/2020JB020430

Chao, K., & Obara, K. (2016, January). Triggered tectonic tremor in various types of fault systems of Japan following the 2012 M_w 8.6 Sumatra earthquake: TRIGGERED TREMOR IN JAPAN. *Journal of Geophysical Research: Solid Earth*, *121*(1), 170–187. doi: 10.1002/2015JB012566

Chao, K., Peng, Z., Gonzalez-Huizar, H., Aiken, C., Enescu, B., Kao, H., ... Matsuzawa, T. (2013, May). A Global Search for Triggered Tremor Following the 2011 Mw 9.0 Tohoku Earthquake. *Bulletin of the Seismological Society of America*, *103*(2B), 1551–1571. doi: 10.1785/0120120171

Chestler, S. R., & Creager, K. C. (2017, December). A Model for Low-Frequency Earthquake Slip. *Geochemistry, Geophysics, Geosystems*, *18*(12), 4690–4708. doi: 10.1002/2017GC007253

Cruz-Atienza, V. M., Villafuerte, C., & Bhat, H. S. (2018, December). Rapid tremor migration and pore-pressure waves in subduction zones. *Nature Communications*, *9*(1). doi: 10.1038/s41467-018-05150-3

Ester, M., Kriegel, H.-P., Sander, J., & Xu, X. (1996). A Density-Based Algorithm for Discovering Clusters in Large Spatial Databases with Noise. *Proceedings of the 2nd International Conference on Knowledge Discovery and Data mining*, 226–231.

Etheridge, M. A., Wall, V. J., Cox, S. F., & Vernon, R. H. (1984, June). High fluid pressures during regional metamorphism and deformation: Implications for mass transport and deformation mechanisms. *Journal of Geophysical Research: Solid Earth*, *89*(B6), 4344–4358. doi: 10.1029/JB089iB06p04344

Evans, J. P., Forster, C. B., & Goddard, J. V. (1997, November). Permeability of fault-related rocks, and implications for hydraulic structure of fault zones. *Journal of Structural Geology*, *19*(11), 1393–1404. doi: 10.1016/S0191-8141(97)00057-6

Eymold, W. K., Walsh, T. B., Moortgat, J., Grove, B. S., & Darrah, T. H. (2021, April). Constraining fault architecture and fluid flow using crustal noble gases. *Applied Geochemistry*, 104954. doi: 10.1016/j.apgeochem.2021.104954

Farge, G., Jaupart, C., & Shapiro, N. M. (2021, September). Episodicity and Migration of Low Frequency Earthquakes Modeled With Fast Fluid Pressure Transients in the Permeable Subduction Interface. *Journal of Geophysical Research: Solid Earth*, *126*(9). doi: 10.1029/2021JB021894

Farge, G., Shapiro, N. M., & Frank, W. B. (2020, August). Moment-Duration Scal-

ing of Low-Frequency Earthquakes in Guerrero, Mexico. *Journal of Geophysical Research: Solid Earth*, *125*(8). doi: 10.1029/2019JB019099

Frank, W. B., & Brodsky, E. E. (2019, October). Daily measurement of slow slip from low-frequency earthquakes is consistent with ordinary earthquake scaling. *Science Advances*, *5*(10), eaaw9386. doi: 10.1126/sciadv.aaw9386

Frank, W. B., Radiguet, M., Rousset, B., Shapiro, N. M., Husker, A. L., Kostoglodov, V., ... Campillo, M. (2015, April). Uncovering the geodetic signature of silent slip through repeating earthquakes: UNCOVERING SILENT SLIP. *Geophysical Research Letters*, *42*(8), 2774–2779. doi: 10.1002/2015GL063685

Frank, W. B., Shapiro, N. M., Husker, A. L., Kostoglodov, V., Bhat, H. S., & Campillo, M. (2015, March). Along-fault pore-pressure evolution during a slow-slip event in Guerrero, Mexico. *Earth and Planetary Science Letters*, *413*, 135–143. doi: 10.1016/j.epsl.2014.12.051

Frank, W. B., Shapiro, N. M., Husker, A. L., Kostoglodov, V., Gusev, A. A., & Campillo, M. (2016, April). The evolving interaction of low-frequency earthquakes during transient slip. *Science Advances*, *2*(4), e1501616. doi: 10.1126/sciadv.1501616

Frank, W. B., Shapiro, N. M., Husker, A. L., Kostoglodov, V., Romanenko, A., & Campillo, M. (2014, October). Using systematically characterized low-frequency earthquakes as a fault probe in Guerrero, Mexico. *Journal of Geophysical Research: Solid Earth*, *119*(10), 7686–7700. doi: 10.1002/2014JB011457

Fukuda, K., Hatano, T., & Mochizuki, K. (2022, January). Model for tectonic tremors: Enduring events, moment rate spectrum, and moment-duration scaling. *Physical Review E*, *105*(1), 014124. doi: 10.1103/PhysRevE.105.014124

Ghosh, A., Vidale, J. E., Sweet, J. R., Creager, K. C., Wech, A. G., Houston, H., & Brodsky, E. E. (2010, December). Rapid, continuous streaking of tremor in Cascadia. *Geochemistry, Geophysics, Geosystems*, *11*(12), n/a-n/a. doi: 10.1029/2010GC003305

Giger, S. B., Tenthorey, E., Cox, S. F., & Fitz Gerald, J. D. (2007, July). Permeability evolution in quartz fault gouges under hydrothermal conditions. *Journal of Geophysical Research*, *112*(B7). doi: 10.1029/2006JB004828

Goh, K.-I., & Barabasi, A.-L. (2006, October). Burstiness and Memory in Complex Systems. *arXiv:physics/0610233*.

Gold, T., & Soter, S. (1985). Fluid ascent through the solid lithosphere and its relation to earthquakes. *Pure and Applied Geophysics PAGEOPH*, *122*(2-4), 492–530. doi: 10.1007/BF00874614

Gosselin, J. M., Audet, P., Estève, C., McLellan, M., Mosher, S. G., & Schaeffer, A. J. (2020, January). Seismic evidence for megathrust fault-valve behavior during episodic tremor and slip. *Science Advances*, *6*(4), eaay5174. doi: 10.1126/sciadv.aay5174

Hall, K., Schmidt, D., & Houston, H. (2019, November). Peak Tremor Rates Lead Peak Slip Rates During Propagation of Two Large Slow Earthquakes in Cascadia. *Geochemistry, Geophysics, Geosystems*, *20*(11), 4665–4675. doi: 10.1029/2019GC008510

Halpaap, F., Rondenay, S., Perrin, A., Goes, S., Ottemöller, L., Austrheim, H., ... Eeken, T. (2019, April). Earthquakes track subduction fluids from slab source to mantle wedge sink. *Science Advances*, *5*(4), eaav7369. doi: 10.1126/sciadv.aav7369

Hayes, G. (2018). *Slab2 - A Comprehensive Subduction Zone Geometry Model.* U.S. Geological Survey. doi: 10.5066/F7PV6JNV

Hubbert, M. K., & Willis, D. G. (1957). Mechanics of Hydraulic Fracturing. *Transactions of the AIME*, *210*, 153–168.

Husker, A., Frank, W. B., Gonzalez, G., Avila, L., Kostoglodov, V., & Kazachkina,

E. (2019, January). Characteristic Tectonic Tremor Activity Observed Over Multiple Slow Slip Cycles in the Mexican Subduction Zone. *Journal of Geophysical Research: Solid Earth*, *124*(1), 599–608. doi: 10.1029/2018JB016517

Hyndman, R. D., McCrory, P. A., Wech, A., Kao, H., & Ague, J. (2015, June). Cascadia subducting plate fluids channelled to fore-arc mantle corner: ETS and silica deposition. *Journal of Geophysical Research: Solid Earth*, *120*(6), 4344–4358. doi: 10.1002/2015JB011920

Ide, S. (2010, July). Striations, duration, migration and tidal response in deep tremor. *Nature*, *466*(7304), 356–359. doi: 10.1038/nature09251

Ide, S. (2019). Detection of Low-Frequency Earthquakes in Broadband Random Time Sequences: Are They Independent Events? *Journal of Geophysical Research: Solid Earth*, *124*(8), 8611–8625. doi: 10.1029/2019JB017643

Ide, S. (2021, December). Empirical Low-Frequency Earthquakes Synthesized From Tectonic Tremor Records. *Journal of Geophysical Research: Solid Earth*, *126*(12). doi: 10.1029/2021JB022498

Ide, S., & Nomura, S. (2022, December). Forecasting tectonic tremor activity using a renewal process model. *Progress in Earth and Planetary Science*, *9*(1), 67. doi: 10.1186/s40645-022-00523-1

Ide, S., Shelly, D. R., & Beroza, G. C. (2007, February). Mechanism of deep low frequency earthquakes: Further evidence that deep non-volcanic tremor is generated by shear slip on the plate interface. *Geophysical Research Letters*, *34*(3). doi: 10.1029/2006GL028890

Ide, S., & Yabe, S. (2014). Universality of slow earthquakes in the very low frequency band. *Geophysical Research Letters*, *41*(8), 2786–2793. doi: 10.1002/2014GL059712

Idehara, K., Yabe, S., & Ide, S. (2014, December). Regional and global variations in the temporal clustering of tectonic tremor activity. *Earth, Planets and Space*, *66*(1), 66. doi: 10.1186/1880-5981-66-66

Im, K., Elsworth, D., & Wang, C. (2019, May). Cyclic Permeability Evolution During Repose Then Reactivation of Fractures and Faults. *Journal of Geophysical Research: Solid Earth*, *124*(5), 4492–4506. doi: 10.1029/2019JB017309

Imanishi, K., Uchide, T., & Takeda, N. (2016). Determination of focal mechanisms of nonvolcanic tremor using S wave polarization data corrected for the effects of anisotropy. *Geophysical Research Letters*, *43*(2), 611–619. doi: 10.1002/2015GL067249

Ito, Y., Obara, K., Shiomi, K., Sekine, S., & Hirose, H. (2007). Slow Earthquakes Coincident with Episodic Tremors and Slow Slip Events. *Science, New Series*, *315*(5811), 503–506.

Iwasaki, T., Sato, H., Ishiyama, T., Shinohara, M., & Hashima, A. (2015). Fundamental structure model of island arcs and subducted plates in and around Japan. In *AGU Fall Meeting Abstracts* (Vol. 2015, p. T31B-2878).

Jäger, R., Mendoza, M., & Herrmann, H. J. (2017, September). The Mechanism behind Erosive Bursts in Porous Media. *Physical Review Letters*, *119*(12), 124501. doi: 10.1103/PhysRevLett.119.124501

Journeau, C., Shapiro, N. M., Seydoux, L., Soubestre, J., Koulakov, I. Y., Jakovlev, A. V., ... Jaupart, C. (2022, February). Seismic tremor reveals active trans-crustal magmatic system beneath Kamchatka volcanoes. *Science Advances*, *8*(5), eabj1571. doi: 10.1126/sciadv.abj1571

Kano, M., Kato, A., Ando, R., & Obara, K. (2018, February). Strength of tremor patches along deep transition zone of a megathrust. *Scientific Reports*, *8*(1), 3655. doi: 10.1038/s41598-018-22048-8

Katsumata, A., & Kamaya, N. (2003, January). Low-frequency continuous tremor around the Moho discontinuity away from volcanoes in the southwest Japan: DEEP TREMOR IN THE SOUTHWEST JAPAN. *Geophysical Research Letters*, *30*(1), 20-1-20-4. doi: 10.1029/2002GL015981

Kostoglodov, V., Husker, A., Shapiro, N. M., Payero, J. S., Campillo, M., Cotte, N., & Clayton, R. (2010). The 2006 slow slip event and nonvolcanic tremor in the Mexican subduction zone. *Geophysical Research Letters*, *37*(24). doi: 10.1029/2010GL045424

Kotowski, A. J., & Behr, W. M. (2019, August). Length scales and types of heterogeneities along the deep subduction interface: Insights from exhumed rocks on Syros Island, Greece. *Geosphere*, *15*(4), 1038–1065. doi: 10.1130/GES02037.1

Kurihara, R., Obara, K., Takeo, A., & Maeda, T. (2018, April). Migration of Deep Low-Frequency Tremor Triggered by Teleseismic Earthquakes in the Southwest Japan Subduction Zone. *Geophysical Research Letters*, *45*(8), 3413–3419. doi: 10.1002/2017GL076779

Luo, Y., & Liu, Z. (2019). Rate-and-State Model Casts New Insight into Episodic Tremor and Slow-slip Variability in Cascadia. *Geophysical Research Letters*, 11.

Masuda, K., Ide, S., Ohta, K., & Matsuzawa, T. (2020, December). Bridging the gap between low-frequency and very-low-frequency earthquakes. *Earth, Planets and Space*, *72*(1), 47. doi: 10.1186/s40623-020-01172-8

Materna, K., Bartlow, N., Wech, A., Williams, C., & Bürgmann, R. (2019, November). Dynamically Triggered Changes of Plate Interface Coupling in Southern Cascadia. *Geophysical Research Letters*, *46*(22), 12890–12899. doi: 10.1029/2019GL084395

Maury, J., Ide, S., Cruz-Atienza, V. M., & Kostoglodov, V. (2018, February). Spatiotemporal Variations in Slow Earthquakes Along the Mexican Subduction Zone. *Journal of Geophysical Research: Solid Earth*, *123*(2), 1559–1575. doi: 10.1002/2017JB014690

McLellan, M., Audet, P., Rosas, J. C., & Currie, C. (2022, December). Margin-wide variations in slab dehydration in Cascadia and their relationship to slow slip. *Lithos*, *434–435*, 106912. doi: 10.1016/j.lithos.2022.106912

Mitchell, T. M., & Faulkner, D. R. (2008, November). Experimental measurements of permeability evolution during triaxial compression of initially intact crystalline rocks and implications for fluid flow in fault zones. *Journal of Geophysical Research*, *113*(B11), B11412. doi: 10.1029/2008JB005588

Miyazawa, M., Brodsky, E. E., & Mori, J. (2008, October). Learning from dynamic triggering of low-frequency tremor in subduction zones. *Earth, Planets and Space*, *60*(10), e17-e20. doi: 10.1186/BF03352858

Muñoz-Montecinos, J., Angiboust, S., Garcia-Casco, A., Glodny, J., & Bebout, G. (2021, March). Episodic hydrofracturing and large-scale flushing along deep subduction interfaces: Implications for fluid transfer and carbon recycling (Zagros Orogen, southeastern Iran). *Chemical Geology*, 120173. doi: 10.1016/j.chemgeo.2021.120173

Nakajima, J., & Hasegawa, A. (2016, December). Tremor activity inhibited by well-drained conditions above a megathrust. *Nature Communications*, *7*(1), 13863. doi: 10.1038/ncomms13863

Nakajima, J., & Uchida, N. (2018, May). Repeated drainage from megathrusts during episodic slow slip. *Nature Geoscience*, *11*(5), 351–356. doi: 10.1038/s41561-018-0090-z

Obara, K. (2002, May). Nonvolcanic Deep Tremor Associated with Subduction in Southwest Japan. *Science*, *296*(5573), 1679–1681. doi: 10.1126/science.1070378

Obara, K., Hirose, H., Yamamizu, F., & Kasahara, K. (2004, December). Episodic slow slip events accompanied by non-volcanic tremors in southwest Japan subduction zone: EPISODIC SLOW SLIP AND TREMOR IN JAPAN. *Geophysical Research Letters*, *31*(23). doi: 10.1029/2004GL020848

Ohmi, S., & Obara, K. (2002, August). Deep low-frequency earthquakes beneath the focal region of the Mw 6.7 2000 Western Tottori earthquake: DLF BE-

NEATH THE FOCAL REGION OF THE 2000 WESTERN TOTTORI EQ. *Geophysical Research Letters*, *29*(16), 54-1-54-4. doi: 10.1029/2001GL014469

Peacock, S. M., Christensen, N. I., Bostock, M. G., & Audet, P. (2011, May). High pore pressures and porosity at 35 km depth in the Cascadia subduction zone. *Geology*, *39*(5), 471–474. doi: 10.1130/G31649.1

Pedregosa, F., Varoquaux, G., Gramfort, A., Michel, V., Thirion, B., Grisel, O., ... Duchesnay, É. (2011). Scikit-learn: Machine Learning in Python. *Journal of Machine Learning Research*, *12*(85), 2825–2830.

Piccoli, F., Ague, J. J., Chu, X., Tian, M., & Brovarone, A. V. (2021, February). Field-based evidence for intra-slab high-permeability channel formation at eclogite-facies conditions during subduction. *Geochemistry, Geophysics, Geosystems*. doi: 10.1029/2020GC009520

Platt, J. P., Xia, H., & Schmidt, W. L. (2018, December). Rheology and stress in subduction zones around the aseismic/seismic transition. *Progress in Earth and Planetary Science*, *5*(1), 24. doi: 10.1186/s40645-018-0183-8

Poiata, N., Vilotte, J.-P., Shapiro, N., Obara, K., & Supino, M. (2021, July). *Low-frequency earthquake catalog for western and central Shikoku, Japan.* doi: 10.31905/UOQ9LVHZ

Poiata, N., Vilotte, J.-P., Shapiro, N. M., Supino, M., & Obara, K. (2021, November). Complexity of Deep Low-Frequency Earthquake Activity in Shikoku (Japan) Imaged From the Analysis of Continuous Seismic Data. *Journal of Geophysical Research: Solid Earth*, *126*(11). doi: 10.1029/2021JB022138

Radiguet, M., Cotton, F., Vergnolle, M., Campillo, M., Walpersdorf, A., Cotte, N., & Kostoglodov, V. (2012). Slow slip events and strain accumulation in the Guerrero gap, Mexico. *Journal of Geophysical Research: Solid Earth*, *117*(B4). doi: 10.1029/2011JB008801

Rogers, G. (2003, June). Episodic Tremor and Slip on the Cascadia Subduction Zone: The Chatter of Silent Slip. *Science*, *300*(5627), 1942–1943. doi: 10.1126/science.1084783

Ross, Z. E., Cochran, E. S., Trugman, D. T., & Smith, J. D. (2020, June). 3D fault architecture controls the dynamism of earthquake swarms. *Science*, *368*(6497), 1357–1361. doi: 10.1126/science.abb0779

Royer, A. A., & Bostock, M. G. (2014, September). A comparative study of low frequency earthquake templates in northern Cascadia. *Earth and Planetary Science Letters*, *402*, 247–256. doi: 10.1016/j.epsl.2013.08.040

Rubin, A. M., & Armbruster, J. G. (2013, December). Imaging slow slip fronts in Cascadia with high precision cross-station tremor locations: IMAGING SLOW SLIP FRONTS IN CASCADIA. *Geochemistry, Geophysics, Geosystems*, *14*(12), 5371–5392. doi: 10.1002/2013GC005031

Rubinstein, J. L., Gomberg, J., Vidale, J. E., Wech, A. G., Kao, H., Creager, K. C., & Rogers, G. (2009, February). Seismic wave triggering of nonvolcanic tremor, episodic tremor and slip, and earthquakes on Vancouver Island. *Journal of Geophysical Research*, *114*, B00A01. doi: 10.1029/2008JB005875

Sammis, C. G., & Bostock, M. G. (2021). A Granular Jamming Model for Low-Frequency Earthquakes. *Journal of Geophysical Research: Solid Earth*, *126*(7), e2021JB021963. doi: 10.1029/2021JB021963

Segall, P., Rubin, A. M., Bradley, A. M., & Rice, J. R. (2010, December). Dilatant strengthening as a mechanism for slow slip events. *Journal of Geophysical Research*, *115*(B12), B12305. doi: 10.1029/2010JB007449

Shapiro, N. M., Campillo, M., Kaminski, E., Vilotte, J.-P., & Jaupart, C. (2018, October). Low-Frequency Earthquakes and Pore Pressure Transients in Subduction Zones. *Geophysical Research Letters*, *45*(20), 11,083–11,094. doi: 10.1029/2018GL079893

Shelly, D. R., Beroza, G. C., & Ide, S. (2007, March). Non-volcanic tremor and low-frequency earthquake swarms. *Nature*, *446*(7133), 305–307. doi: 10.1038/

nature05666

Shelly, D. R., Beroza, G. C., Ide, S., & Nakamula, S. (2006, July). Low-frequency earthquakes in Shikoku, Japan, and their relationship to episodic tremor and slip. *Nature*, *442*(7099), 188–191. doi: 10.1038/nature04931

Shillington, D. J., Bécel, A., Nedimović, M. R., Kuehn, H., Webb, S. C., Abers, G. A., ... Mattei-Salicrup, G. A. (2015, December). Link between plate fabric, hydration and subduction zone seismicity in Alaska. *Nature Geoscience*, *8*(12), 961–964. doi: 10.1038/ngeo2586

Sibson, R. (1992, September). Implications of fault-valve behaviour for rupture nucleation and recurrence. *Tectonophysics*, *211*(1-4), 283–293. doi: 10.1016/0040-1951(92)90065-E

Sibson, R. H. (2017, December). Tensile overpressure compartments on low-angle thrust faults. *Earth, Planets and Space*, *69*(1), 113. doi: 10.1186/s40623-017-0699-y

Souzy, M., Zuriguel, I., & Marin, A. (2020, June). Transition from clogging to continuous flow in constricted particle suspensions. *Physical Review E*, *101*(6), 060901. doi: 10.1103/PhysRevE.101.060901

Steinwinder, J., & Beckingham, L. E. (2019, July). Role of Pore and Pore-Throat Distributions in Controlling Permeability in Heterogeneous Mineral Dissolution and Precipitation Scenarios. *Water Resources Research*, *55*(7), 5502–5517. doi: 10.1029/2019WR024793

Supino, M., Poiata, N., Festa, G., Vilotte, J. P., Satriano, C., & Obara, K. (2020, April). Self-similarity of low-frequency earthquakes. *Scientific Reports*, *10*(1), 1–9. doi: 10.1038/s41598-020-63584-6

Sweet, J. R., Creager, K. C., Houston, H., & Chestler, S. R. (2019, February). Variations in Cascadia Low-Frequency Earthquake Behavior With Downdip Distance. *Geochemistry, Geophysics, Geosystems*, *20*(2), 1202–1217. doi: 10.1029/2018GC007998

Taetz, S., John, T., Bröcker, M., Spandler, C., & Stracke, A. (2018, January). Fast intraslab fluid-flow events linked to pulses of high pore fluid pressure at the subducted plate interface. *Earth and Planetary Science Letters*, *482*, 33–43. doi: 10.1016/j.epsl.2017.10.044

Takei, Y., & Kumazawa, M. (1994, July). Why have the single force and torque been excluded from seismic source models? *Geophysical Journal International*, *118*(1), 20–30. doi: 10.1111/j.1365-246X.1994.tb04672.x

Tanaka, Y., Suzuki, T., Imanishi, Y., Okubo, S., Zhang, X., Ando, M., ... Hiraoka, Y. (2018, December). Temporal gravity anomalies observed in the Tokai area and a possible relationship with slow slips. *Earth, Planets and Space*, *70*(1), 25. doi: 10.1186/s40623-018-0797-5

Tarling, M. S., Smith, S. A., Rooney, J. S., Viti, C., & Gordon, K. C. (2021, June). A common type of mineralogical banding in serpentine crack-seal veins. *Earth and Planetary Science Letters*, *564*, 116930. doi: 10.1016/j.epsl.2021.116930

Tarling, M. S., Smith, S. A. F., & Scott, J. M. (2019, December). Fluid overpressure from chemical reactions in serpentinite within the source region of deep episodic tremor. *Nature Geoscience*, *12*(12), 1034–1042. doi: 10.1038/s41561-019-0470-z

Tenthorey, E., & Cox, S. F. (2006). Cohesive strengthening of fault zones during the interseismic period: An experimental study. *Journal of Geophysical Research*, *111*(B9), B09202. doi: 10.1029/2005JB004122

Ukawa, M., & Ohtake, M. (1987). A monochromatic earthquake suggesting deep-seated magmatic activity beneath the Izu-Ooshima Volcano, Japan. *Journal of Geophysical Research*, *92*(B12), 12649. doi: 10.1029/JB092iB12p12649

Wang, K., & Bilek, S. L. (2014, January). Invited review paper: Fault creep caused by subduction of rough seafloor relief. *Tectonophysics*, *610*, 1–24. doi: 10.1016/j.tecto.2013.11.024

Wang, T., Zhuang, J., Buckby, J., Obara, K., & Tsuruoka, H. (2018, August). Identifying the Recurrence Patterns of Nonvolcanic Tremors Using a 2-D Hidden Markov Model With Extra Zeros. *Journal of Geophysical Research: Solid Earth*. doi: 10.1029/2017JB015360

Wannamaker, P. E., Evans, R. L., Bedrosian, P. A., Unsworth, M. J., Maris, V., & McGary, R. S. (2014, November). Segmentation of plate coupling, fate of subduction fluids, and modes of arc magmatism in Cascadia, inferred from magnetotelluric resistivity. *Geochemistry, Geophysics, Geosystems*, *15*(11), 4230–4253. doi: 10.1002/2014GC005509

Warren-Smith, E., Fry, B., Wallace, L., Chon, E., Henrys, S., Sheehan, A., ... Lebedev, S. (2019, May). Episodic stress and fluid pressure cycling in subducting oceanic crust during slow slip. *Nature Geoscience*, 1. doi: 10.1038/s41561-019-0367-x

Wech, A. G., & Creager, K. C. (2007, November). Cascadia tremor polarization evidence for plate interface slip. *Geophysical Research Letters*, *34*(22), L22306. doi: 10.1029/2007GL031167

Wech, A. G., & Creager, K. C. (2008, October). Automated detection and location of Cascadia tremor. *Geophysical Research Letters*, *35*(20), L20302. doi: 10.1029/2008GL035458

Wech, A. G., & Creager, K. C. (2011, September). A continuum of stress, strength and slip in the Cascadia subduction zone. *Nature Geoscience*, *4*(9), 624–628. doi: 10.1038/ngeo1215

Wech, A. G., Thelen, W. A., & Thomas, A. M. (2020, May). Deep long-period earthquakes generated by second boiling beneath Mauna Kea volcano. *Science*, *368*(6492), 775–779. doi: 10.1126/science.aba4798

Yamazaki, T., & Okamura, Y. (1989, March). Subducting seamounts and deformation of overriding forearc wedges around Japan. *Tectonophysics*, *160*(1), 207–229. doi: 10.1016/0040-1951(89)90392-2

Yasuhara, H., & Elsworth, D. (2008, July). Compaction of a Rock Fracture Moderated by Competing Roles of Stress Corrosion and Pressure Solution. *Pure and Applied Geophysics*, *165*(7), 1289–1306. doi: 10.1007/s00024-008-0356-2

Figure 1.

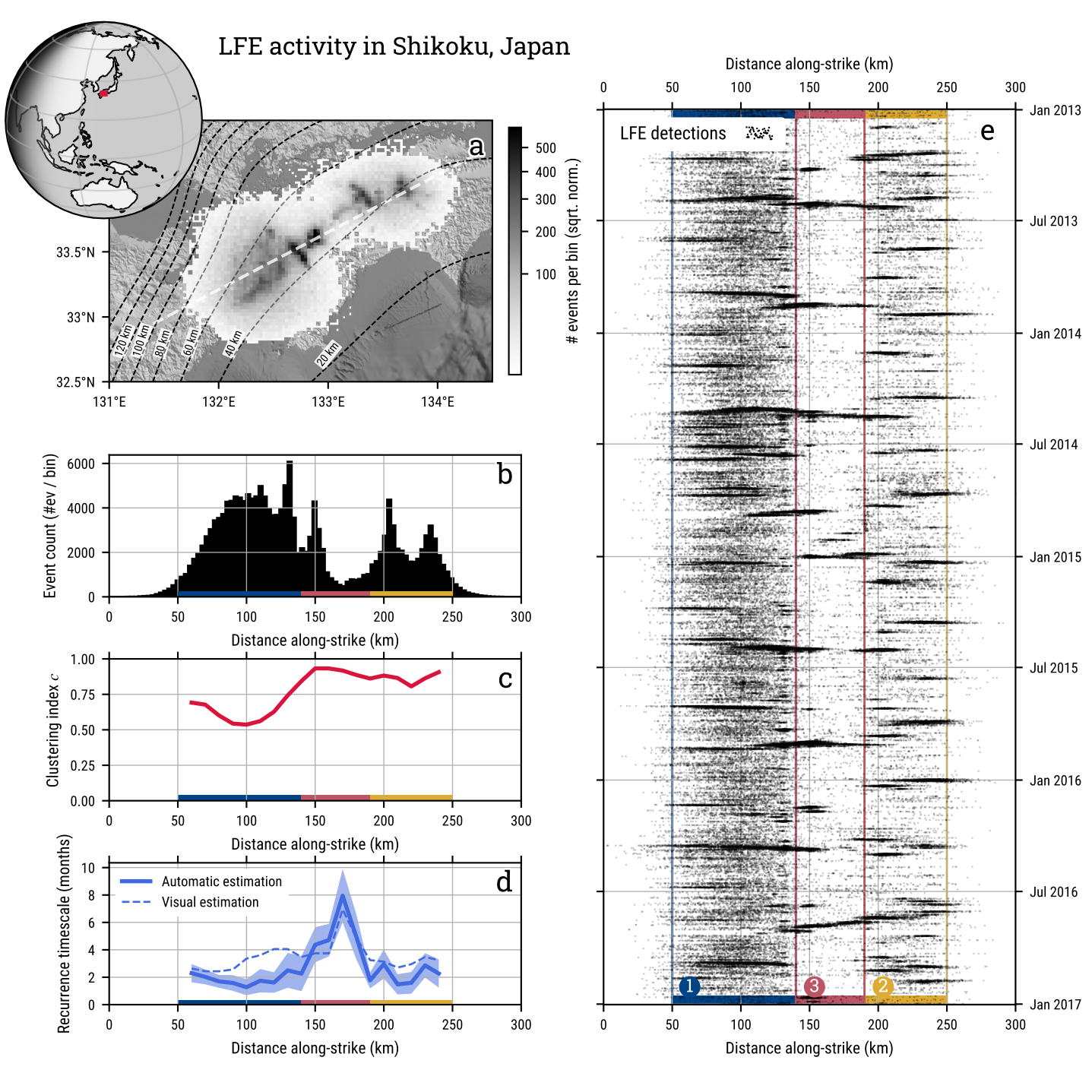
LFE activity in Shikoku, Japan
a
33.5°N
33°N
32.5°N
131°E
132°E
133°E
134°E
120 km
100 km
80 km
60 km
40 km
20 km
500
400
300
200
100
events per bin (sqrt. norm.)
b
Event count (#ev / bin)
6000
4000
2000
0
Distance along-strike (km)
c
Clustering index c
1.00
0.75
0.50
0.25
0.00
Distance along-strike (km)
d
Recurrence timescale (months)
Automatic estimation
Visual estimation
Distance along-strike (km)
e
LFE detections
Distance along-strike (km)
Jan 2013
Jul 2013
Jan 2014
Jul 2014
Jan 2015
Jul 2015
Jan 2016
Jul 2016
Jan 2017
1
3
2

Figure 2.

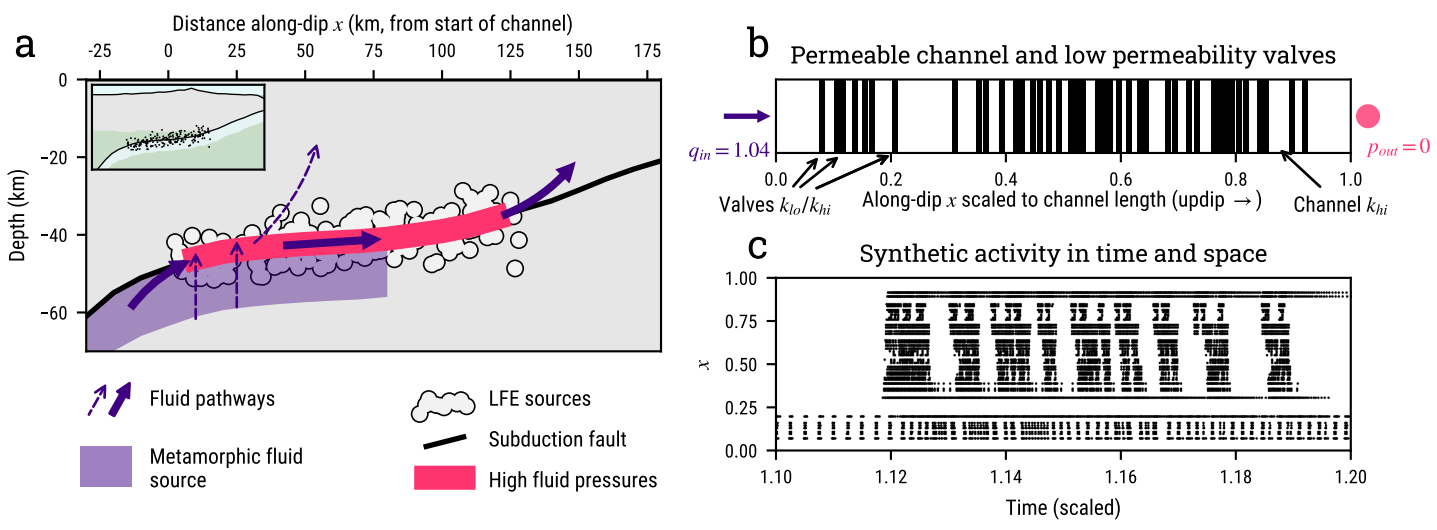
a
Distance along-dip x (km, from start of channel)
-25
0
25
50
75
100
125
150
175
Depth (km)
0
-20
-40
-60
Fluid pathways
Metamorphic fluid source
LFE sources
Subduction fault
High fluid pressures
b
Permeable channel and low permeability valves
$q_{in} = 1.04$
$p_{out} = 0$
0.0
0.2
0.4
0.6
0.8
1.0
Valves k_{lo}/k_{hi}
Along-dip x scaled to channel length (updip →)
Channel k_{hi}
c
Synthetic activity in time and space
x
1.00
0.75
0.50
0.25
0.00
1.10
1.12
1.14
1.16
1.18
1.20
Time (scaled)

Figure 3.

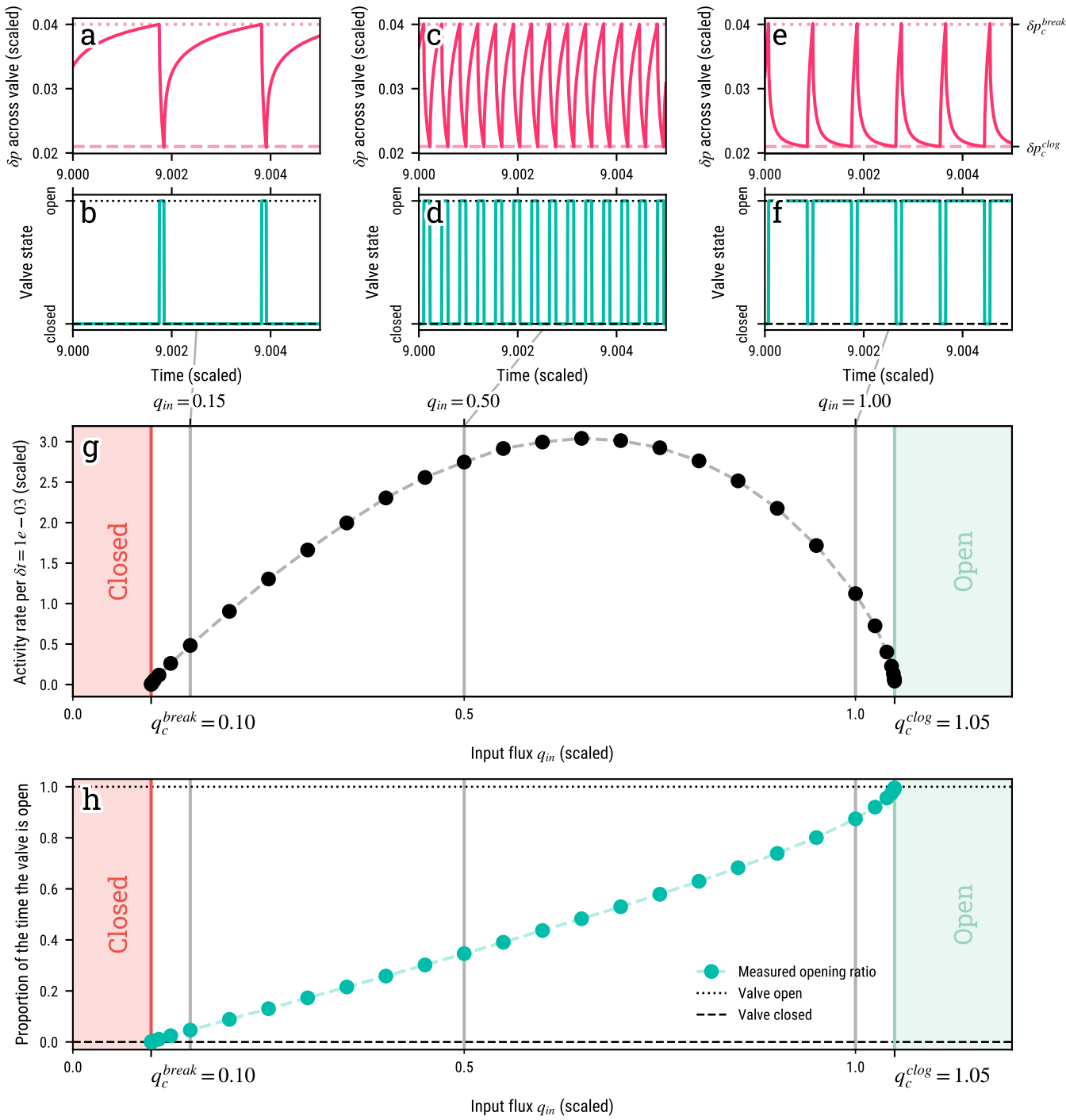
Temporal behavior of a single valve for different values of the input flux q_{in}
a
b
c
d
e
f
g
h
δp across valve (scaled)
Valve state
open
closed
Time (scaled)
$q_{in} = 0.15$
$q_{in} = 0.50$
$q_{in} = 1.00$
δp_c^{break}
δp_c^{clog}
Activity rate per $\delta t = 1e-03$ (scaled)
Proportion of the time the valve is open
Closed
Open
$q_c^{break} = 0.10$
$q_c^{clog} = 1.05$
Input flux q_{in} (scaled)
Measured opening ratio
Valve open
Valve closed

Figure 4.

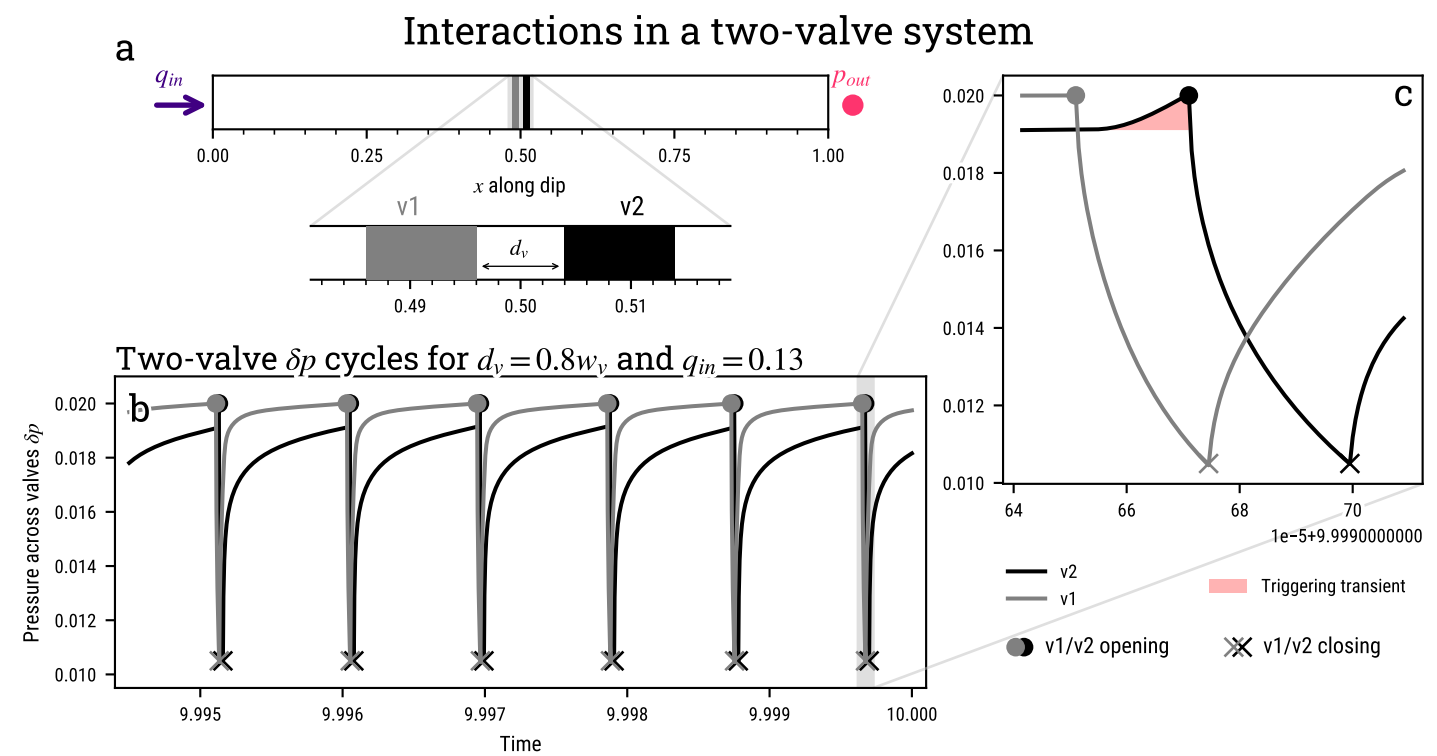
Interactions in a two-valve system
a
q_{in}
p_{out}
0.00
0.25
0.50
0.75
1.00
x along dip
v1
v2
d_v
0.49
0.50
0.51
Two-valve δp cycles for $d_v = 0.8 w_v$ and $q_{in} = 0.13$
b
Pressure across valves δp
0.020
0.018
0.016
0.014
0.012
0.010
9.995
9.996
9.997
9.998
9.999
10.000
Time
c
0.020
0.018
0.016
0.014
0.012
0.010
64
66
68
70
1e−5+9.9990000000
v2
v1
Triggering transient
v1/v2 opening
v1/v2 closing

Figure 5.

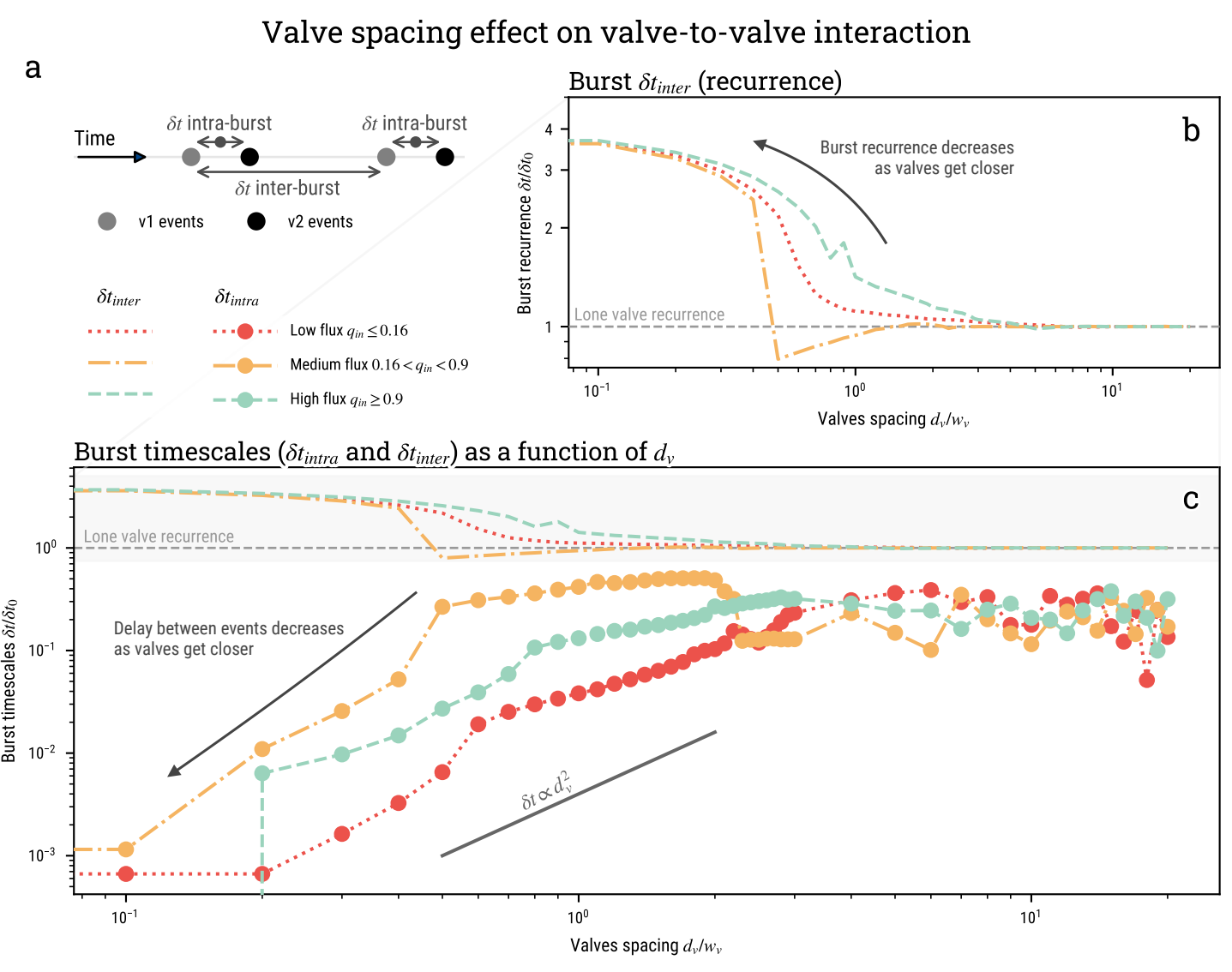
Valve spacing effect on valve-to-valve interaction
a
Time
δt intra-burst
δt intra-burst
δt inter-burst
v1 events
v2 events
δt_inter
δt_intra
Low flux q_in ≤ 0.16
Medium flux 0.16 < q_in < 0.9
High flux q_in ≥ 0.9
Burst δt_inter (recurrence)
b
Burst recurrence decreases as valves get closer
Lone valve recurrence
Burst recurrence δt/δt0
Valves spacing d_v/w_v
Burst timescales (δt_intra and δt_inter) as a function of d_v
c
Lone valve recurrence
Delay between events decreases as valves get closer
δt ∝ d_v^2
Burst timescales δt/δt0
Valves spacing d_v/w_v

Figure 6.

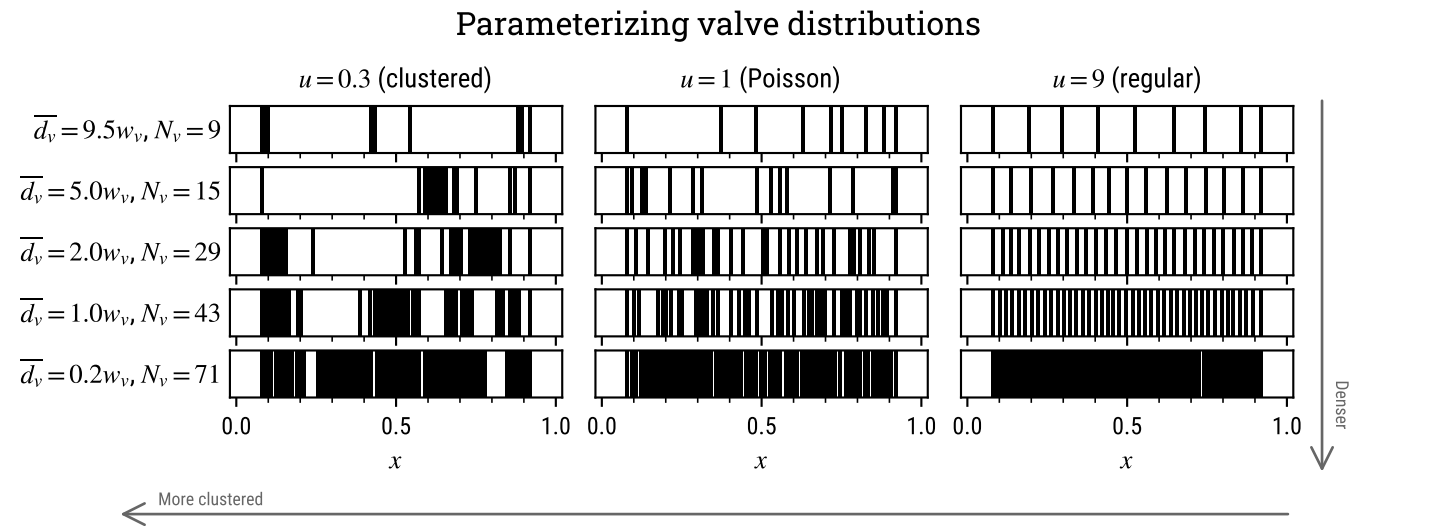
Parameterizing valve distributions
$u = 0.3$ (clustered)
$u = 1$ (Poisson)
$u = 9$ (regular)
$\overline{d_v} = 9.5 w_v$, $N_v = 9$
$\overline{d_v} = 5.0 w_v$, $N_v = 15$
$\overline{d_v} = 2.0 w_v$, $N_v = 29$
$\overline{d_v} = 1.0 w_v$, $N_v = 43$
$\overline{d_v} = 0.2 w_v$, $N_v = 71$
0.0
0.5
1.0
x
Denser
More clustered

Figure 7.

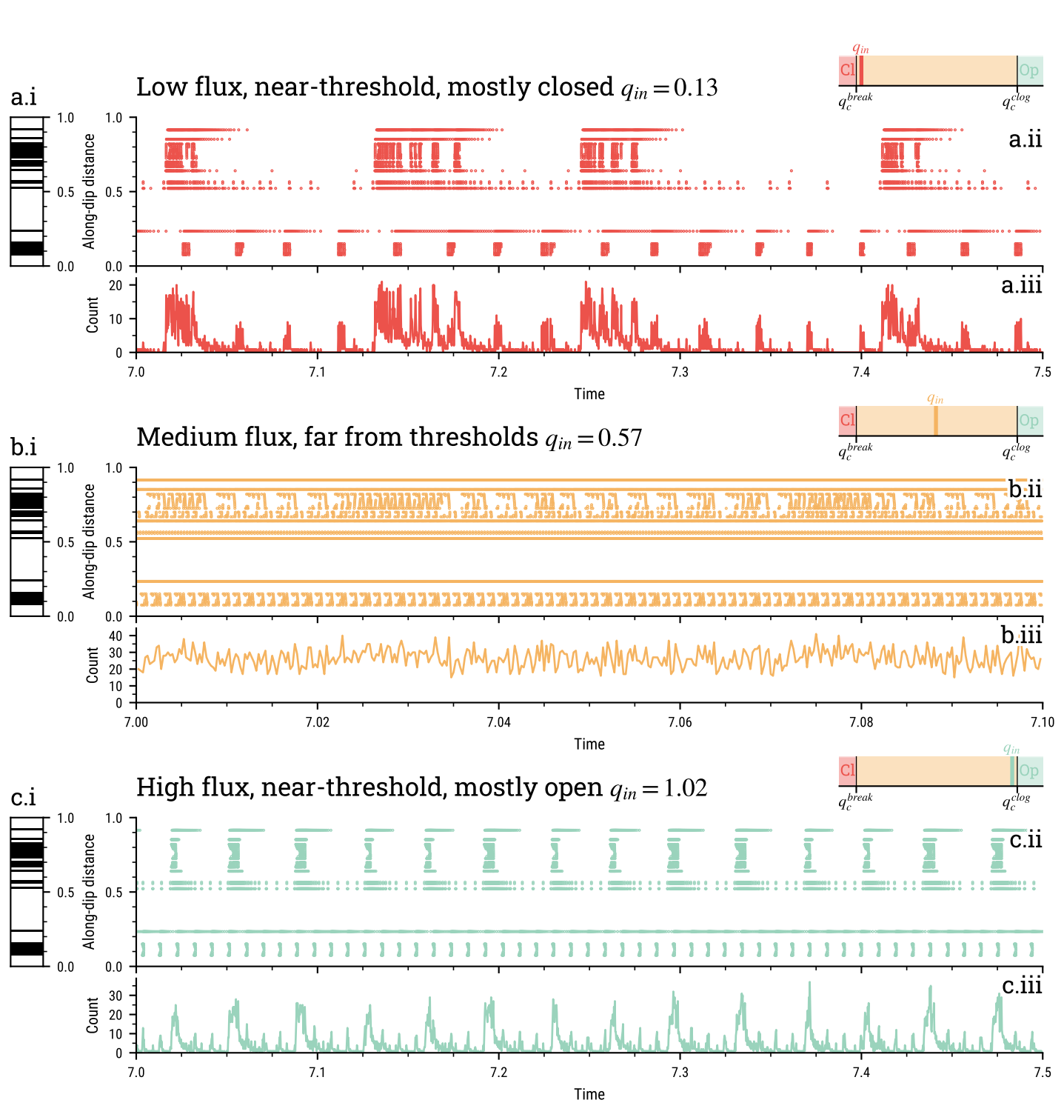
a.i
Low flux, near-threshold, mostly closed $q_{in} = 0.13$
q_{in}
Cl
Op
q_c^{break}
q_c^{clog}
a.ii
a.iii
Along-dip distance
Count
Time
b.i
Medium flux, far from thresholds $q_{in} = 0.57$
b.ii
b.iii
c.i
High flux, near-threshold, mostly open $q_{in} = 1.02$
c.ii
c.iii

Figure 8.

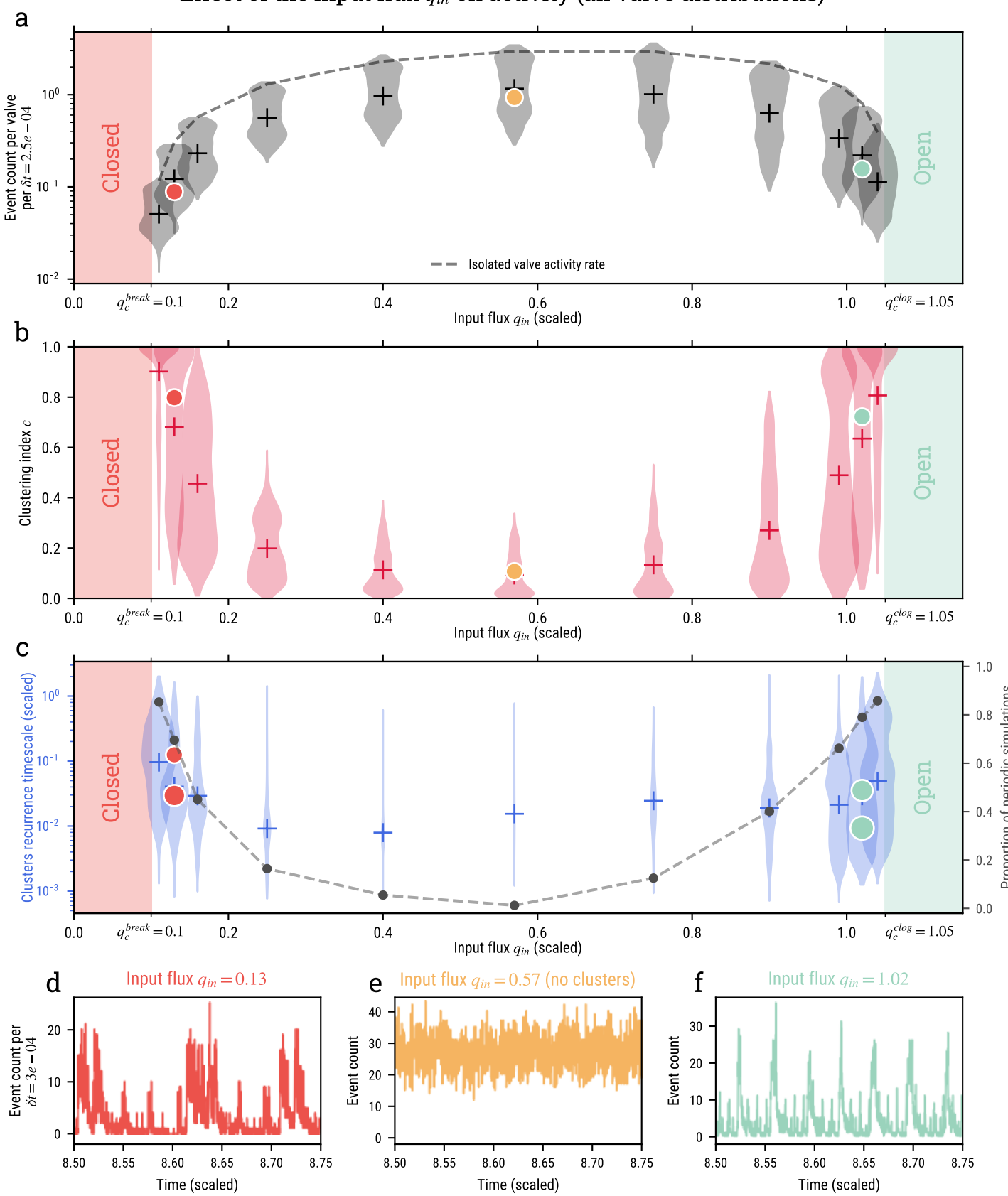
Effect of the input flux q_{in} on activity (all valve distributions)
a
Event count per valve per $\delta t = 2.5e-04$
Closed
Open
Isolated valve activity rate
Input flux q_{in} (scaled)
$q_c^{break} = 0.1$
$q_c^{clog} = 1.05$
b
Clustering index c
Closed
Open
Input flux q_{in} (scaled)
c
Clusters recurrence timescale (scaled)
Proportion of periodic simulations
Closed
Open
Input flux q_{in} (scaled)
d
Input flux $q_{in} = 0.13$
Event count per $\delta t = 3e-04$
Time (scaled)
e
Input flux $q_{in} = 0.57$ (no clusters)
Event count
Time (scaled)
f
Input flux $q_{in} = 1.02$
Event count
Time (scaled)

Figure 9.

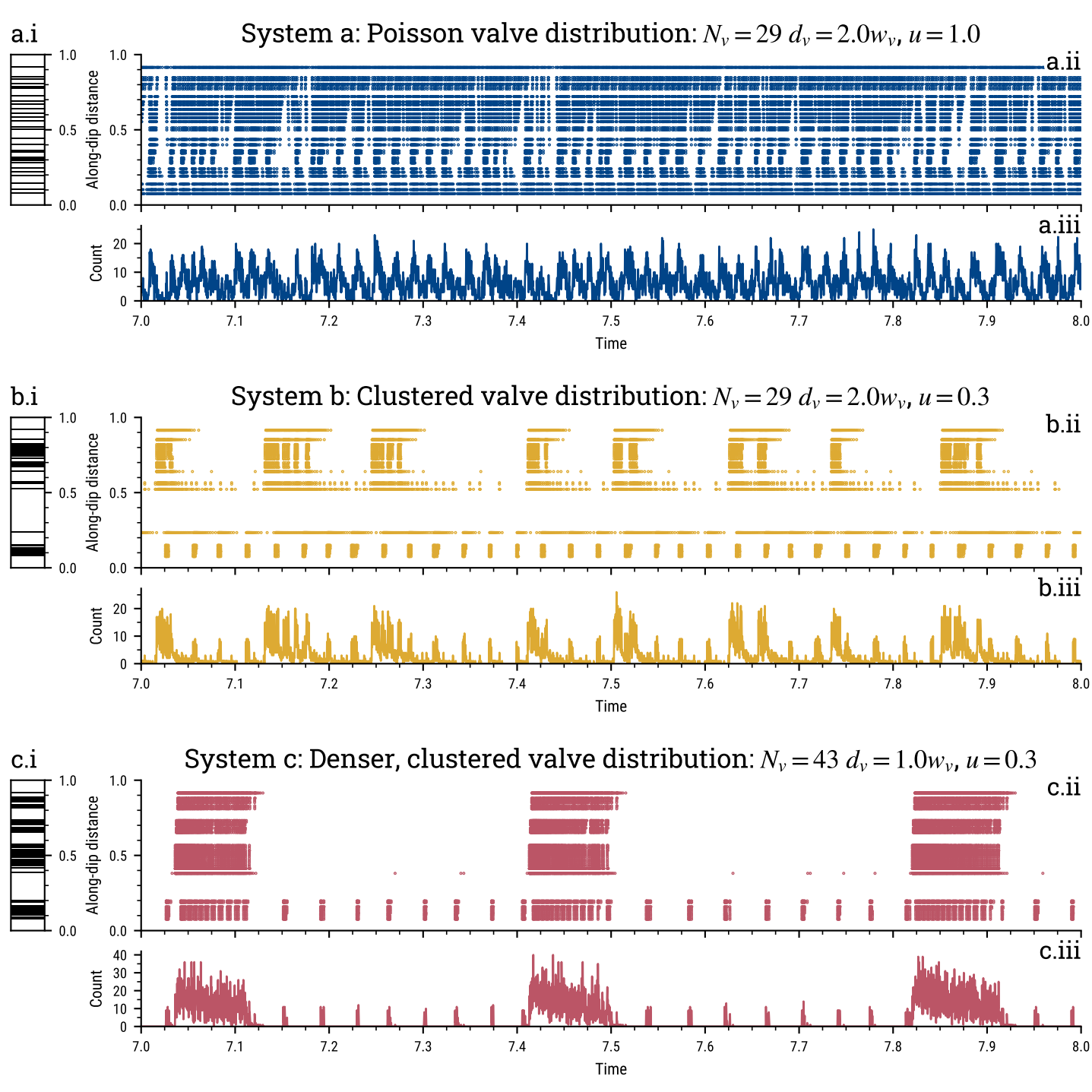
a.i
System a: Poisson valve distribution: $N_v = 29$ $d_v = 2.0w_v$, $u = 1.0$
a.ii
a.iii
Along-dip distance
Count
Time
b.i
System b: Clustered valve distribution: $N_v = 29$ $d_v = 2.0w_v$, $u = 0.3$
b.ii
b.iii
Along-dip distance
Count
Time
c.i
System c: Denser, clustered valve distribution: $N_v = 43$ $d_v = 1.0w_v$, $u = 0.3$
c.ii
c.iii
Along-dip distance
Count
Time

Figure 10.

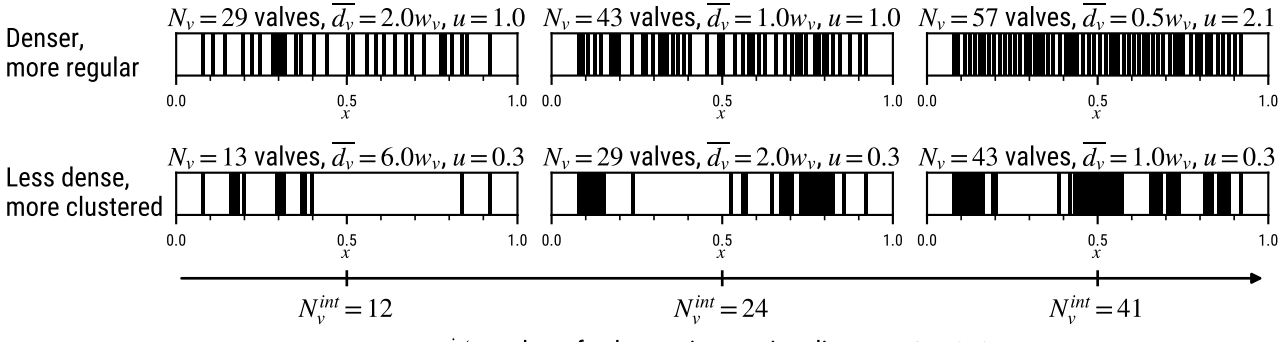
Parameterizing valve proximity
Denser, more regular
Less dense, more clustered
$N_v = 29$ valves, $\overline{d_v} = 2.0w_v$, $u = 1.0$
$N_v = 43$ valves, $\overline{d_v} = 1.0w_v$, $u = 1.0$
$N_v = 57$ valves, $\overline{d_v} = 0.5w_v$, $u = 2.1$
$N_v = 13$ valves, $\overline{d_v} = 6.0w_v$, $u = 0.3$
$N_v = 29$ valves, $\overline{d_v} = 2.0w_v$, $u = 0.3$
$N_v = 43$ valves, $\overline{d_v} = 1.0w_v$, $u = 0.3$
0.0
0.5
1.0
x
$N_v^{int} = 12$
$N_v^{int} = 24$
$N_v^{int} = 41$
N_v^{int} number of valves at interacting distance $d_v < 0.5w_v$

Figure 11.

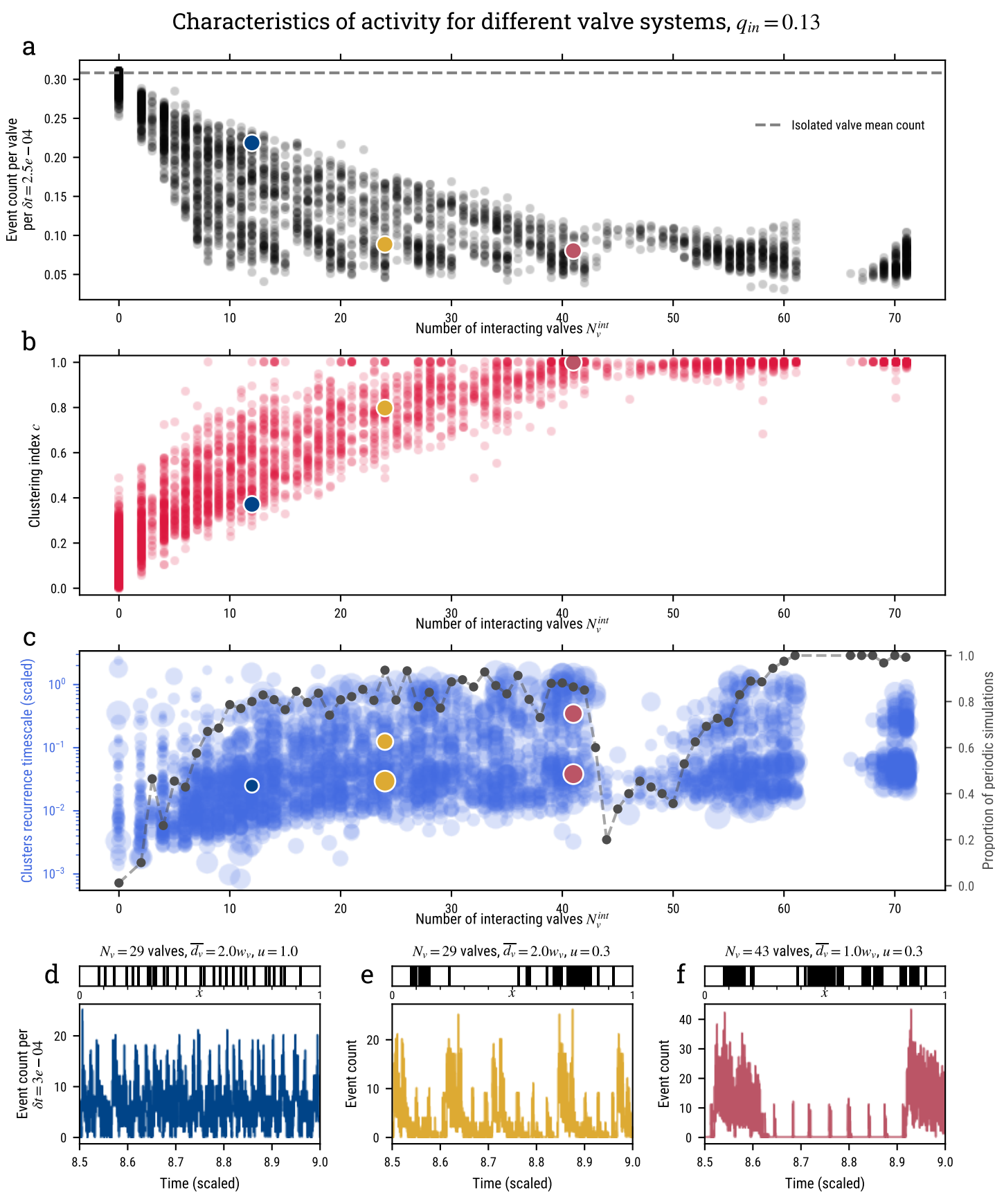
Characteristics of activity for different valve systems, $q_{in} = 0.13$
a
Event count per valve per $\delta t = 2.5e-04$
Isolated valve mean count
Number of interacting valves N_v^{int}
b
Clustering index c
Number of interacting valves N_v^{int}
c
Clusters recurrence timescale (scaled)
Proportion of periodic simulations
Number of interacting valves N_v^{int}
$N_v = 29$ valves, $\overline{d_v} = 2.0 w_v$, $u = 1.0$
d
Event count per $\delta t = 3e-04$
Time (scaled)
$N_v = 29$ valves, $\overline{d_v} = 2.0 w_v$, $u = 0.3$
e
Event count
Time (scaled)
$N_v = 43$ valves, $\overline{d_v} = 1.0 w_v$, $u = 0.3$
f
Event count
Time (scaled)

Figure 12.

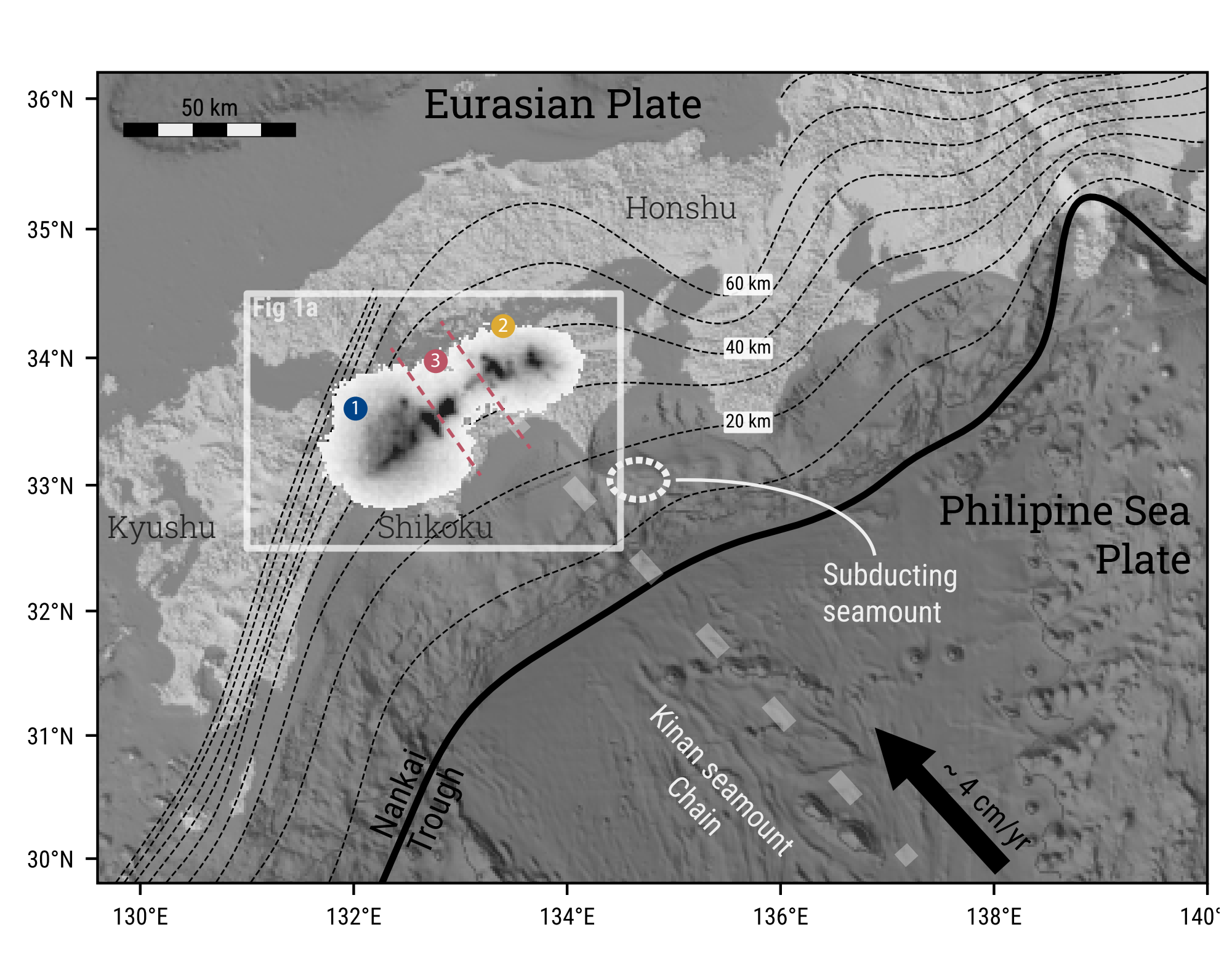
Eurasian Plate
50 km
Honshu
60 km
40 km
20 km
Fig 1a
1
2
3
Kyushu
Shikoku
Philipine Sea Plate
Subducting seamount
Kinan seamount Chain
Nankai Trough
~ 4 cm/yr
36°N
35°N
34°N
33°N
32°N
31°N
30°N
130°E
132°E
134°E
136°E
138°E
140°